

Probabilistic Forecasting of the Arctic Sea Ice Edge with Contour Modeling¹

Hannah M. Director
Department of Statistics
University of Washington

Adrian E. Raftery
Departments of Statistics and Sociology
University of Washington

Cecilia M. Bitz
Department of Atmospheric Sciences
University of Washington

November 15, 2022

¹The authors thank Nicholas Wayand for assistance with data processing and Arlan Dirkson for addressing questions on trend adjusted quantile mapping. All authors were supported by NOAA's Climate Program Office, Climate Variability and Predictability Program through grant NA15OAR4310161. HMD was also supported by the National Science Foundation Graduate Research Fellowship under Grant No. DGE-1256082. All results in this paper were produced using the *IceCast* R package (Director et al., 2019) and code which can be accessed at <https://github.com/hdirector/ProbSeaIce>.

Abstract

Sea ice, or frozen ocean water, annually freezes and melts in the Arctic. The need for accurate forecasts of where sea ice will be located weeks to months in advance has increased as the amount of sea ice reduces due to climate change. Typical sea ice forecasts are made with ensemble models, physics-based deterministic models of sea ice and the surrounding ocean and atmosphere. This paper introduces Mixture Contour Forecasting, a method to forecast sea ice that post-processes output from ensembles and weights them with observed sea ice patterns in recent years. These forecasts are better calibrated than unadjusted dynamic ensemble forecasts and other statistical reference forecasts. To produce these forecasts, a novel statistical technique is introduced that directly models the sea ice edge contour, the boundary around the region that is ice-covered. Most of the computational effort in post-processing can therefore be placed on the sea ice edge contour, which is of particular importance due to its role in maritime planning. Mixture Contour Forecasting and reference methods are evaluated for monthly sea ice forecasts for 2008-2016 at lead times ranging from 0.5-6.5 months using the European Centre for Medium-Range Weather Forecasts ensemble.

Keywords: spatiotemporal, climate change, forecasting, post-processing, mixtures.

Contents

1	Introduction	1
2	A general contour model	3
2.1	Notation and setup	3
2.2	Bayesian model	6
2.2.1	Parametric covariance	6
2.2.2	Prior distribution	7
2.2.3	Posterior distribution	8
3	Post-processing ensemble forecasts	9
3.1	Review of Contour-Shifting	10
3.2	Calibrating the ensemble by generating contours	11
3.3	Mixture Contour Forecasting	11
4	Method evaluation	13
4.1	Evaluation set-up	13
4.2	Forecast Assessment	16
5	Discussion	19
A	Standard deviation corresponding to γ proportion of mass of a Gaussian within symmetric bounds	26
B	Posterior distribution given partially observed X	26
C	Additional figures	27
D	MCMC Algorithm	31
D.1	Metropolis step for each $x_{ij}^u \in \mathbf{X}^u$	31
D.2	Gibbs step for μ	31
D.3	Metropolis steps for σ	32
D.4	Metropolis step for ρ	32
D.5	Initialization	33
D.6	Implementation	34
E	MCMC diagnostics	34
E.1	Sample Evaluation: September 2005	34
F	Length of Training Periods	39

List of Tables

1	Summary of forecasts types evaluated. Probabilistic forecasts give estimates in the interval $[0, 1]$ and binary forecasts indicate predicted sea ice presence	15
2	The 50-th, 85-th, and 100-th percentile for the estimated chain lengths for μ_i obtained from the Raftery and Lewis Diagnostic for the three regions evaluated.	35
3	As in Table 2, except for σ_i	35
4	Estimated chain lengths from the Raftery and Lewis Diagnostic for ρ	35
5	Mean area-weighted Brier scores for MCF on the test set of 2012-2016 for different numbers of years of training data are used to determine the weight on the climatology versus the post-processed ensemble.	40

List of Figures

1	The average proportion of times sea ice was observed, plotted against the predicted probability of observing sea ice for the unadjusted ECMWF ensemble forecasts (left) and for the corresponding Mixture Contour Forecasts (right) for lead times of 0.5 to 1.5 months. Results are for September 2008-2016. A perfectly calibrated forecast would have all points on the $y = x$ line, so the MCF is better calibrated.	2
2	Arctic ocean regions used in this analysis. Each region in a color other than beige is fit with a contour model. The bold lines in all regions except the Central Arctic are the fixed set of boundary points \mathbf{B} , connected with a line. The ‘+’ symbol denotes the location of \mathbf{B} in the Central Arctic Region. Areas in grey are land and areas in white are ocean regions that are not considered part of the Arctic.	4
3	Hypothetical sea ice edge contours (\mathbf{S}), fixed boundaries (\mathbf{B}), bounding locations (\mathbf{M}), and parallel lines (\mathbf{L}) on which the points $s \in \mathbf{S}$ will be generated for an example typical region (left) and for the Central Arctic region (right). The green line designates the observed length for the 14th (left) and 57th (right) lines.	5
4	The posterior probability of observing sea ice in September fit from observations from 1998-2007. The red lines bound the 95% interval. The black lines show the ten contours used to fit the model. The observed contours are most often found within areas with high probability and are rarely found outside the 95% interval bounds. Small areas of sea ice can be observed away from the main sea ice region and accounting for them will be addressed in Section 3.3.	9
5	Weight on the post-processed ensemble model by month and lead time. A black dot indicates that the weight is at least 0.4. The post-processed ensemble gets more weight at short lead times and in the months leading up to the sea ice minimum. The weight on climatology is equal to one minus the weight on the post-processed ensemble.	13
6	Forecasts of the probability of sea ice presence for September 2008 using different methods. Forecasts are described in Table 1. The red line is the observed sea ice edge contour and white areas are land. For MCF, the observed ice edge is almost completely within areas with positive probability and has little area where sea ice is predicted with probability 1, but is not observed. In contrast, the observed sea ice edge more often goes through regions with zero probability in the ensemble and post-processed ensemble forecasts. In the climatology forecast, there is considerable area where sea ice is predicted with probability 1 but is not observed.	17

7	Plots of the average proportion of times sea ice was observed against predicted probability of sea ice presence for the raw ECMWF forecasts (left) and after post-processing with MCF (middle) and TAQM (right). Forecasts are grouped into lead times of 0.5 and 1.5 months (top) and 2.5-6.5 months (bottom). A perfectly calibrated forecast would have all points on the $y = x$ line.	18
8	Average Brier scores by month for the test years 2008-2016 for the probabilistic forecasts and a damped persistence reference binary forecast. The Brier Score for each grid box is weighted based on its area. Forecasts are described in Table 1. . .	19
9	As in Figure 8, but for the binary forecasts.	20
10	Overall Brier scores for the test years 2008-2016 for the probabilistic forecasts and a damped persistence reference binary forecast. The Brier Score for each grid box is weighted based on its area. Forecasts are described in Table 1 in the main text. . . .	27
11	Average Brier scores grouped into three-month sets for the test years 2008-2016 for the probabilistic forecasts and a damped persistence reference binary forecast. The Brier Score for each grid box is weighted based on its area. Forecasts are described in Table 1 in the main text.	28
12	As in Figure 11, except for binary forecasts.	28
13	Plots of the average proportion of times sea ice was observed against the predicted probability of observing sea ice for the unadjusted ECMWF forecasts (top) and post-processed with MCF (middle) and TAQM (bottom) for lead times of 0.5 - 1.5 months. Results are grouped into three-month sets and all grid boxes are equally weighted.	29
14	As in Figure 13 but for lead times of 2.5 - 6.5 months.	30
15	Traceplots for the chains in each of the three evaluated regions for a typical μ_i . . .	36
16	Traceplots for the chains in each of the three evaluated regions for a typical σ_i . . .	37
17	Traceplots for the parameter ρ in the three evaluated regions.	38

1 Introduction

With anthropogenic climate change, rapid changes have been observed in the Arctic. Among these changes has been a substantial reduction in the area of the ocean’s surface that freezes. Sea ice, or frozen ocean water, annually freezes and melts in response to seasonal changes in atmospheric and oceanic processes. Since the the satellite record began in 1979, the amount of sea ice in the Arctic has rapidly declined (Comiso et al., 2008; Stroeve et al., 2012). Continued reduction in sea ice is expected as the effects of climate changes increase. Reduced sea ice cover allows for increased Arctic shipping (Smith and Stephenson, 2013; Melia et al., 2016). The importance of forecasting sea ice has increased in response, since waters without sea ice are more easily navigable than waters with sea ice. With accurate sea ice forecasts, maritime routes can be selected that avoid sea ice.

Sea ice concentration, or the percent of ice-covered area, has been observed for a little over 40 years and is available on a grid. For navigational purposes, the concentration field can be reduced to a binary field indicating the presence or absence of sea ice. Prediction efforts then focus on the location of the ice edge contour, or boundary line that separates ice-covered regions and open water. A grid box is typically considered ice-covered if its concentration is at least 15%. Results are not particularly sensitive to this threshold, since the transition from high to low concentration is rapid.

Zhang and Cressie (2019) have introduced a hierarchical spatio-temporal generalized linear model for Arctic sea ice. However, many sea ice forecasts used in practice are informed by numerical prediction systems. These systems are deterministic, and they integrate systems of differential equations to represent the physical processes that drive sea ice formation and melting. These systems are typically run multiple times with slightly-different initial conditions. Since the modeled processes are chaotic, the resulting runs have varying sea ice. The collection of forecasts, referred to as the ensemble, has shown skill in predicting the total area or extent of sea ice at seasonal time scales in retrospective forecasts (e.g., Sigmond et al., 2013; Msadek et al., 2014; Wang et al., 2013; Chevallier et al., 2013) and in current forecasts (Blanchard-Wrigglesworth et al., 2015). Skill has also been shown at regional scales (Bushuk et al., 2017) and for spatial fields for some models at short lead times (Zampieri et al., 2018). However, errors in ensembles are common because the underlying systems of differential equations are only approximations of the true physical processes, and because initial conditions are insufficiently known given chaotic error growth (Guemas et al., 2016; Blanchard-Wrigglesworth et al., 2015). Ensembles can be biased and/or improperly calibrated, meaning that the mean behavior of the ensemble is systematically incorrect and/or the range of possible sea ice states predicted by the ensemble members does not reflect the

actual uncertainty of the forecast.

Statistical post-processing, or methods to adjust ensemble forecasts, can be applied to address ensembles’ errors while maintaining much of the skill they provide. In this paper, we develop Mixture Contour Forecasting (MCF), a post-processing method to improve the calibration of sea ice forecasts. We develop a way to generate distributions of sea ice edge contours that is used in conjunction with a previously-developed bias correction technique for the ice edge, called Contour-Shifting (Director et al., 2017). The forecasts from the generated contour distributions are weighted with climatological information to account for the time-varying skill of ensemble forecasts and aspects of sea ice that cannot be represented well with a contour model, such as holes in the ice. The MCF method provides better calibrated and generally more accurate forecasts than the unadjusted ensemble, existing post-processing techniques, and statistical reference forecasts. In Figure 1, we illustrate the extent to which MCF improves model calibration by plotting the predicted probability of sea ice presence in September against the actual proportion of times sea ice was observed for the raw ensemble and after post-processing. The predictions are for the European Centre for Medium-Range Weather Forecasts (ECMWF) ensemble forecast. We see that MCF dramatically improves model calibration.

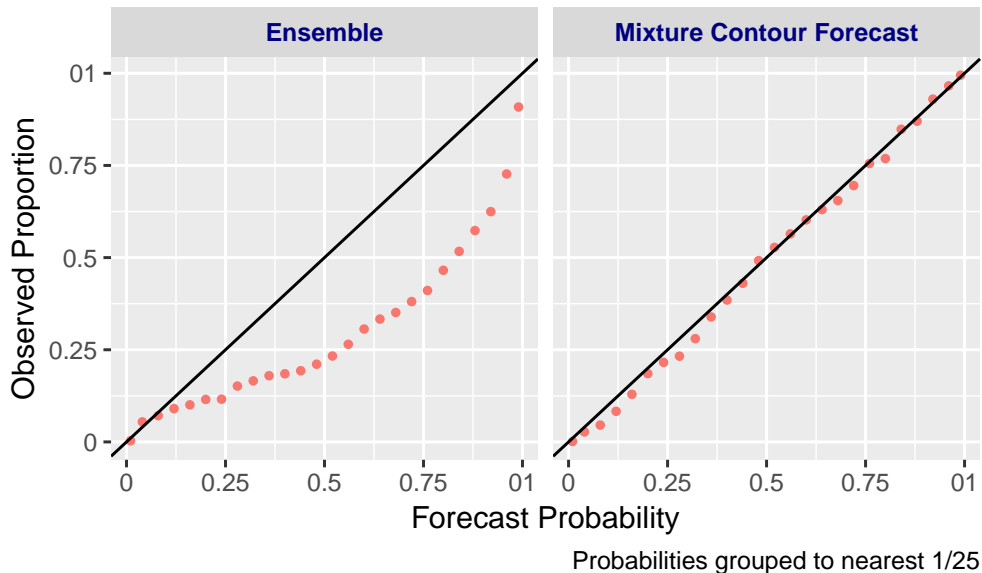


Figure 1: The average proportion of times sea ice was observed, plotted against the predicted probability of observing sea ice for the unadjusted ECMWF ensemble forecasts (left) and for the corresponding Mixture Contour Forecasts (right) for lead times of 0.5 to 1.5 months. Results are for September 2008-2016. A perfectly calibrated forecast would have all points on the $y = x$ line, so the MCF is better calibrated.

The paper is organized as follows. In Section 2, we introduce a contour model for the sea ice edge. In Section 3, we discuss post-processing of the ensemble and how we combine this with climatological information to implement MCF. We also briefly review the Contour-Shifting bias correction method introduced in Director et al. (2017). In Section 4, we compare the performance of our post-processing techniques to other post-processing and statistical forecasting techniques. In Section 5, we conclude with discussion.

2 A general contour model

We first introduce how to define and generate a distribution of realistic ice edge contours by directly modeling a contour as a sequence of connected points. We initially focus on a purely statistical model, e.g., a model based only on sea ice observations, but in subsequent sections we will use this model as a basis for statistical post-processing of the output of ensemble forecasting systems.

2.1 Notation and setup

A contour is the boundary line enclosing a defined area, which in this case is the region that contains sea ice. A contour, denoted \mathbf{S} , can be represented as an ordered sequence of n spatial points, (S_1, \dots, S_n) , where each S_i is an (x, y) coordinate pair. Connecting S_i to S_{i+1} for all $i = 1, \dots, n-1$ and S_n to S_1 encloses an area. Following this definition, to generate a distribution of contours we need a way to generate realizations of \mathbf{S} . While the sea ice edge is colloquially referred to as a singular entity, it is actually a collection of edges defining multiple contiguous areas of sea ice.

We will model the sea ice edge for seven regions individually. These seven regions, shown in the map in Figure 2, exclude parts of the Arctic where a contour model is not optimal. The remaining regions will be addressed separately in Section 3.3. We selected these regions by modifying an existing region mask (Cavalieri and Parkinson, 2012) obtained from the National Snow and Ice Data Center (2017). Regions were generally modified from the original mask when multiple non-contiguous sections of sea ice were expected within a region. We refer to the sea ice edge contour in a given region simply as \mathbf{S} .

In most regions, sea ice is formed in contiguous sections bordering land. In these regions, \mathbf{S} is formed by a sequence of points that proceed from the coastline, into the ocean, and back to the coastline. We can reduce the number of points that need to be estimated by fixing a set of boundary points, $\mathbf{B} = (B_1, \dots, B_n)$ on land and considering how far into the ocean the contour extends at each boundary location. To do this, we lay out an ordered series of



Figure 2: Arctic ocean regions used in this analysis. Each region in a color other than beige is fit with a contour model. The bold lines in all regions except the Central Arctic are the fixed set of boundary points \mathbf{B} , connected with a line. The ‘+’ symbol denotes the location of \mathbf{B} in the Central Arctic Region. Areas in grey are land and areas in white are ocean regions that are not considered part of the Arctic.

parallel lines, $\mathbf{L} = (L_1, \dots, L_n)$, that cover the region and assume that one point, S_i , lies on each line, L_i . The angle of these lines is set to approximately match the direction the sea ice grows off the land in each region. We denote the length of the line from each point on the coastline, B_i , to the corresponding S_i as y_i . The set of all line lengths is denoted by $Y = (y_1, \dots, y_n)$. The left panel of Figure 3 illustrates these values for the Bering sea.

Unlike in other regions, sea ice in the Central Arctic region is not generally formed off a particular land boundary. To represent the Central Arctic’s contour, we fix all the lines in \mathbf{L} to originate from a single fixed central point rather than from a sequence of points. So, for this region $B_i = B_j$ for all $B_i, B_j \in \mathbf{B}$. The lines extend at fixed angles evenly spaced around a circle as illustrated in the right panel of Figure 3.

Note that given \mathbf{B} , Y , and the angle of \mathbf{L} , we have enough information to identify each S_i , so we need only develop a statistical model for Y to generate contours since \mathbf{B} and \mathbf{L}

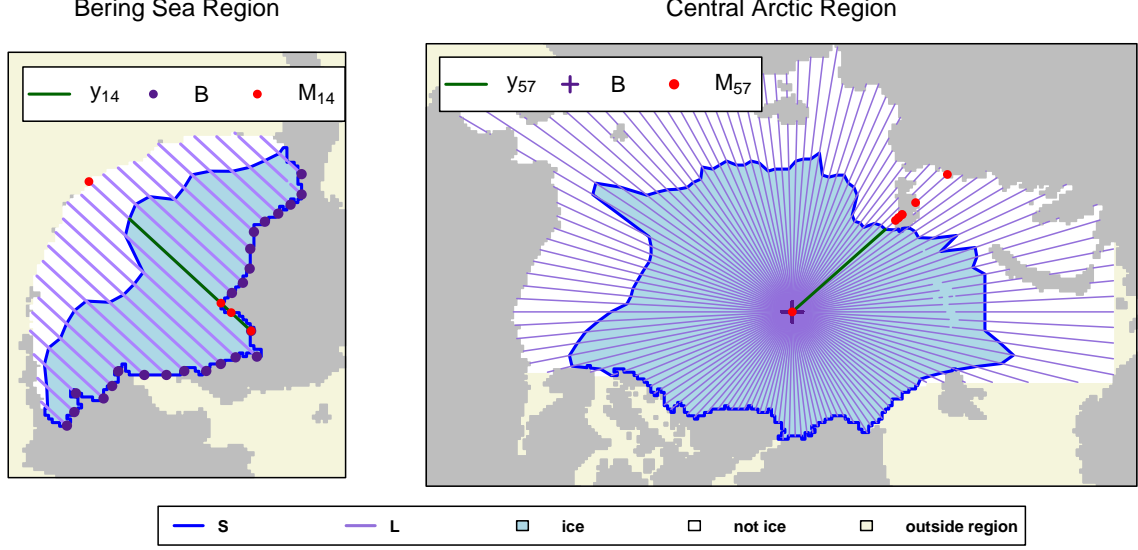


Figure 3: Hypothetical sea ice edge contours (\mathbf{S}), fixed boundaries (\mathbf{B}), bounding locations (\mathbf{M}), and parallel lines (\mathbf{L}) on which the points $s \in \mathbf{S}$ will be generated for an example typical region (left) and for the Central Arctic region (right). The green line designates the observed length for the 14th (left) and 57th (right) lines.

are fixed. In sea ice observations, both the mean and the covariance of y_i values within and across regions varies substantially. To represent these features well, we need a statistical model with a reasonably flexible covariance structure. Modeling Y with a multivariate Gaussian distribution therefore seems natural. However, since y_i is a length contained within a region, the values it can take on are bounded. Additionally, some L_i overlap land, which further restricts the set of possible values that the y_i 's can take. So, direct modeling of Y with a Gaussian distribution is not possible, since random variables drawn from a Gaussian distribution are unbounded. Instead we define Y as a truncated version of some underlying random vector X that follows a multivariate normal distribution. Using this truncation approach maintains many of the desirable features of modeling with a multivariate Gaussian distribution while respecting the constraints on each y_i .

Let $M_i = (m_1, \dots, m_{k_i})$ be a set of k_i lengths that define the boundaries imposed on y_i by L_i . Sample values of M are given in Figure 3. For an L_i that does not cross land, $M_i = (0, \|L_i\|)$, i.e. no line or a line that extends the full length of L_i . For each additional time L_i crosses over land, two additional values are added to M_i , one for the length at which L_i first intersects with the land and another for the length at which the intersection ends. When the generated x_i is within the allowed lengths, $y_i = x_i$. Otherwise, y_i is assigned to the value of m_k that minimizes the distance between it and x_i . More formally, with $k \neq 1, k \neq k_i$,

and k even,

$$y_i|x_i = \begin{cases} 0 & x_i < 0 \\ m_k & m_k \leq x_i \leq m_k + \frac{m_{k+1}-m_k}{2} \\ m_{k+1} & m_k - \frac{m_{k+1}-m_k}{2} \leq x_i \leq m_{k+1} \\ m_{k_i} & x_i > m_{k_i} \\ x_i & \text{otherwise.} \end{cases} \quad (1)$$

This set up has similarities to the Tobit model and its extensions (Tobin, 1958).

The data generating process for \mathbf{S} is simple. First an underlying random vector is drawn where

$$X \sim N(\mu, \Sigma), \quad (2)$$

μ is an $n \times 1$ mean vector and Σ is an $n \times n$ covariance matrix. Once X is drawn, each element in Y is determined from Equation 1. Any y_i that is less than 12.5 (half the nominal length of a grid box) is also set to zero. Rounding in this way provides a better match between the generated data and observations that cannot take on small, non-zero values because of the grid. Each y_i is converted to a location S_i using information about its corresponding L_i . Connecting the values S_i sequentially creates a generated contour. In some places the resulting generated contour line may intersect itself. We correct these intersections with iterative application of the Douglas Peucker algorithm (Douglas and Peucker, 1973). As in Director et al. (2017), we strategically remove the minimum number of generated S_i that cause self-intersections while preserving the general direction of the contour.

2.2 Bayesian model

2.2.1 Parametric covariance

To efficiently fit a model for Equation 2, we define a parametric covariance structure. As noted previously, the variances of y_i are quite varied both within and across regions. However, as for most spatial variables, the values of y_i tend to be more similar when they are closer together. We find that a heterogenous AR(1) covariance,

$$\Sigma = \Sigma(\sigma, \rho) = \begin{bmatrix} \sigma_1^2 & \sigma_1\sigma_2\rho^{d_{12}} & \dots & \sigma_1\sigma_n\rho^{d_{n1}} \\ \sigma_2\sigma_1\rho^{d_{21}} & \sigma_2^2 & \dots & \sigma_2\sigma_n\rho^{d_{2n}} \\ \vdots & \vdots & \ddots & \vdots \\ \sigma_n\sigma_1\rho^{d_{n1}} & \sigma_n\sigma_2\rho^{d_{n2}} & \dots & \sigma_n^2 \end{bmatrix}, \quad (3)$$

(Wolfinger, 1996) is generally flexible enough to capture this behavior. Here $d_{ij} = |i - j|$, ρ is a region-wide correlation parameter, and σ_i^2 is the variance for y_i . We denote $\sigma = (\sigma_1, \dots, \sigma_n)$ for convenience.

In the Central Arctic regions, the lines are laid out in a circle so that the first and last line are physically close to each other despite their indices being far apart. At the loop-over point in the indices, the proposed definition of d_{ij} may appear problematic; however, there is an area above portions of the Canadian Archipelago and Greenland which in all observations is entirely ice-covered. The corresponding variances of the y_i in this area are estimated to be zero regardless of d_{ij} . So, we enumerate L in the Central Arctic such that the loop-over point occurs in this area. The discrepancy between the d_{ij} values and the physical distance therefore does not matter in this area since σ_i and σ_j are estimated to be zero at this location. Since correlation declines with distance, effects of the circular structure farther from the loop-over point are minor. Another way to address the circular structure would be explore correlation structures for spheres such as in Gneiting (2013).

2.2.2 Prior distribution

We take a Bayesian approach to parameter fitting. Since we will combine this statistical model with the ensemble, we use vague priors. While many physical processes controlling sea ice are well-understood, information about these processes is already encoded in a sophisticated way in the ensemble. So, what remains to be modeled statistically is typically poorly understood. We do, however, make use of physical constraints, such as region boundaries and coastlines.

Following these principles, for the parameter vector μ we use the prior distribution

$$\mu \sim N(\mu_0, \mathbf{\Lambda}_0), \quad (4)$$

where μ_0 is a $n \times 1$ mean vector with $\mu_{0,i} = ||L_i||/2$ for all i and $\mathbf{\Lambda}_0$ is a $n \times n$ diagonal covariance matrix with $\mathbf{\Lambda}_{0,ii} = (((||L_i||)/2)/\Phi^{-1}(0.9))^2$ for all i . These parameters set each x_i at the mid-point of L_i and put 80% of the mass in the interval $(0, ||L_i||)$. The value Λ_{ii} is computed using the result in Appendix A with $M = ||L_i||$, $m = 0$, and $\gamma = 0.8$. The variance parameter choice represents our prior belief that most y_i values are not truncated. Since standard deviation values are bounded below and considerable differences in variances exist for the y_i values within Y , we select an independent uniform prior for each σ_i such that

$$p(\sigma_i) \stackrel{iid}{\sim} \text{Unif}(\epsilon, b_0). \quad (5)$$

where $\epsilon = 0.01$ in our implementation.

We bound σ at ϵ rather than zero to avoid numerical issues when σ approaches zero. We also let

$$b_0 = \frac{||L_i||/2}{\Phi^{-1}(0.995)}. \quad (6)$$

The upper bound corresponds to the standard deviation of a Gaussian distribution with 99% of the mass in the interval $(0, ||L_i||)$. The bound is obtained using Appendix A with $M = ||L_i||$, $m = 0$, and $\gamma = 0.99$. Finally, we use a standard non-informative prior for ρ ,

$$p(\rho) \sim \text{Unif}(0, 1). \quad (7)$$

2.2.3 Posterior distribution

We model the columns in $\mathbf{X} = (X_1, \dots, X_N)$ as exchangeable. From each observed contour, we can find all elements Y_j ; however, elements in X_j are only partially known given an observed contour. When $y_{ij} \neq m_k$ for all k we know that x_{ij} has not been truncated. Hence, x_{ij} is known and equals y_{ij} . When $y_{ij} = m_k$ for any k , we do not know the exact value of x_{ij} , but from Equation 1, we can determine in which interval x_{ij} lies. Specifically, with $k \neq 1$, $k \neq k_i$ and k even,

$$x_{ij}|y_{ij} = \begin{cases} (-\infty, 0] & y_{ij} = 0 \\ [m_k, m_k + \frac{m_{k+1}-m_k}{2}] & y_{ij} = m_k \\ [m_k - \frac{m_{k+1}-m_k}{2}, m_{k+1}] & y_{ij} = m_{k+1} \\ [m_{k_i}, \infty) & y_{ij} = m_{k_i} \end{cases} \quad (8)$$

Let \mathbf{X}^o and \mathbf{X}^u denote the observed and unobserved portions of \mathbf{X} respectively. The likelihood for these partially-observed data and the prior distributions introduced in Section 2.2.2 give the posterior distribution

$$\begin{aligned} \prod_{j=1}^N \{p(X_j|\mu, \sigma, \rho)\} p(\mu)p(\sigma)p(\rho) &= \prod_{j=1}^N N(X_j|\mu, \Sigma(\sigma, \rho))N(\mu|\mu_0, \Lambda_0) \times \\ &\quad \prod_{j=1}^N \{\text{Unif}(\sigma_j|\epsilon, b_0)\} \text{Unif}(\rho|0, 1). \end{aligned} \quad (9)$$

See Appendix A for the derivation of this result.

We fit this model for each region independently with Markov chain Monte Carlo (MCMC) using the observed sea ice in the preceding ten years. Regions that are either completely filled with sea ice or contain no sea ice in all training years are omitted from the model fitting. In such cases we predict complete ice-cover or no sea ice respectively. We use Metropolis steps for sampling the values in \mathbf{X}^u , σ , and ρ and a Gibbs step for sampling μ . Detailed information on the sampler and MCMC diagnostics are given in Appendices D and E. Once the model has been fit, we can generate Y values using the mean values from the samples of μ and Σ obtained through the MCMC for the parameters in Equations 2 and 3.

We find that the resulting generated contours approximate the sea ice edge contours observed during the training period. Figure 4 shows the posterior probability of sea ice

presence for the model fit with data for September 1998-2007. The ten observed sea ice edge contours for this period are plotted on top for comparison. The observed contours generally go through regions of high posterior probability and rarely go outside the 95% interval, indicating a good model fit. Of particular note is the model’s ability to capture how the variance changes spatially.

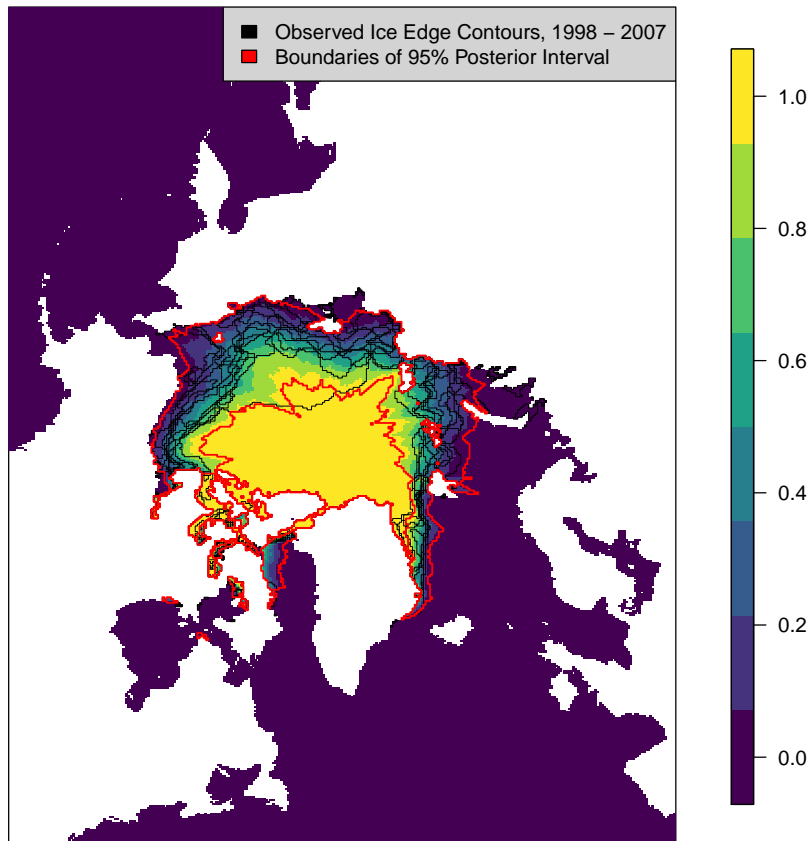


Figure 4: The posterior probability of observing sea ice in September fit from observations from 1998-2007. The red lines bound the 95% interval. The black lines show the ten contours used to fit the model. The observed contours are most often found within areas with high probability and are rarely found outside the 95% interval bounds. Small areas of sea ice can be observed away from the main sea ice region and accounting for them will be addressed in Section 3.3.

3 Post-processing ensemble forecasts

The method in Section 2 generates a distribution of realistic sea ice edge contours that represents the range of possible contours. However, the distributions’s accuracy is limited to that of average behavior in the recent past. In contrast, the ensemble forecast system

can make use of initial conditions and a numerical representation of the physical processes governing sea ice behavior to issue forecasts that are skillful beyond average behavior. The skill of the ensemble, though, is limited by biases and by calibration errors, meaning that the ensemble has systematic errors and its spread does not match observed variability.

A natural path to improve the accuracy of the ensemble is to combine its strengths with that of the contour model. Post-processing takes in the ensemble as an input and adjusts it with a statistical model to remove biases and improve calibration. In this section, we introduce a way to post-process the contour predicted from the ensemble mean. We correct biases in the contours using the previously-developed method of Contour-Shifting and adjust model calibration using the contour model we developed in Section 2. We then introduce MCF, which weights the contour post-processed results with climatology (or average sea ice behavior in recent observations). Weights are selected to reflect the changing skill of the post-processed ensemble for different months and lead times.

3.1 Review of Contour-Shifting

To bias correct the sea ice edge, we largely follow the Contour-Shifting approach introduced in Director et al. (2017). We briefly summarize this approach here and discuss a minor difference in its implementation in this paper. In Director et al. (2017) a bias correction model is fit by comparing the sea ice edge contours in retrospective ensemble mean forecasts to the observed ice edge contours. In each region except the central Arctic, we fix some number of points primarily on land and then evenly space the same number of points on the predicted or observed sea ice edge. We then sequentially connect each point on land to the corresponding point on the sea ice edge. Repeating this process over the training period gives a set of vectors for both the ensemble forecasts and for observations. The components of these sets of vectors can be analyzed to identify systematic differences between the observations and the mean ensemble predictions.

In the central Arctic, we use a simpler approach. We fix a set of lines extending from a point within the interior of the region, as in the right panel of Figure 3. For each observation and ensemble forecast in the training period, we record how far along each line sea ice extends. In this paper, we opt to apply the simpler approach used in the central Arctic region in Director et al. (2017) to all regions. Rather than define the vectors' directions based on the sea ice edge, we only record how far the sea ice extends along the lines \mathbf{L} with fixed direction. Contour-shifting is then easily compatible with the contour model proposed in Section 2, reducing computation.

Following Director et al. (2017), we record how far sea ice extends on each L_i in the training period. We then estimate the length the sea ice will extend to, \hat{w}_i , at some new

time point t for the observations

$$\hat{w}_{i,obs} = \hat{\alpha}_{i,obs} + \hat{\beta}_{i,obs}t, \quad (10)$$

and for the ensemble

$$\hat{w}_{i,dyn} = \hat{\alpha}_{i,dyn} + \hat{\beta}_{i,dyn}t. \quad (11)$$

These regressions are fit using Huber M-estimation, a form of robust linear regression (Huber, 2011). The difference between $\hat{w}_{i,obs} - \hat{w}_{i,dyn}$ gives the expected difference between the length predicted by the mean ensemble and the length that will be observed. We can remove this expected error from the corresponding lengths on the mean ensemble contour forecast to produce a bias-corrected forecast of the mean location of the sea ice edge.

3.2 Calibrating the ensemble by generating contours

The contour model fit in Section 2 accurately describes the variability around the mean sea ice edge contour, while the bias-corrected ensemble mean contour provides information about where the sea ice edge is expected to be. Combining this information allows for forecasts that are more accurate and better calibrated than the ensemble. We combine this information by replacing μ in the statistical model with the lengths of how far sea ice should extend on the lines L in the bias-corrected ensemble mean contour. Then we generate contours as in Section 2 with the covariance fit from observations in recent years. In this approach, the location of the center of distributions of ice-edge contours is controlled by the bias-corrected ensemble, while the variability about this model is informed by a statistical model fit to observations. We refer to forecasts of this form as the post-processed ensemble.

3.3 Mixture Contour Forecasting

The post-processed ensemble forecasts of the sea ice edge generally improve on the raw ensemble. However, they have two main weaknesses. The first is that these forecasts are restricted to be contours. While the vast majority of the sea ice is contained within contiguous areas within the main sea ice edge, small areas of sea ice sometimes still form away from this main area. Areas of open water, called polynyas, also sometimes form as holes within the main sea ice area. Secondly, post-processing only improves an existing ensemble forecast, so if the ensemble forecast is poor, there are limits to how much post-processing can improve it.

MCF corrects these weaknesses. MCF works by weighting the post-processed forecasts with (recent) climatology. Here, we define climatology as the proportion of times sea ice

has been observed in each grid box in the ten years preceding the forecast year. Weights are selected for each forecast month and lead time individually to account for how the post-processed forecasts skill varies based on these factors. The weighting of the post-processed forecast and climatology can be viewed as a simple case of ensemble Bayesian Model Averaging (Raftery et al., 2005).

For a particular forecast month and lead time the weight is fit with maximum likelihood using observations and predictions from preceding years. Let w be the weight on the post-processed ensemble and $1 - w$ be the weight on the climatology. Also, let the variable $\gamma_{s,t}$ be a binary indicator of whether sea ice was observed for some grid box s and year t in the training period. Let $g_p(\gamma_{s,t}|f_{p,s,t})$ and $g_c(\gamma_{s,t}|f_{c,s,t})$ be the corresponding conditional Bernoulli probability of observing the value $\gamma_{s,t}$ given that the probability obtained from the post-processed ensemble or climatology was correct. Assuming that errors in space and time are independent, the corresponding log-likelihood is

$$l(w) = \sum_t \sum_s \log\{w a_s g_p(\gamma_{s,t}|f_{p,s,t}) + (1 - w) a_s g_c(\gamma_{s,t}|f_{c,s,t})\} \quad (12)$$

where a_s is the proportion of the total area in grid box s . Assuming spatial and temporal independence is almost certainly inaccurate; however, Raftery et al. (2005) show in a similar case that weights are not particularly sensitive to this assumption.

To maximize this log-likelihood we use the Expectation-Maximization algorithm (Dempster et al., 1977). We introduce the latent variable $z_{p,s,t}$, which has value 1 if the post-processed ensemble is the best forecast for grid box s in year t and 0 otherwise. The variable $z_{c,s,t}$ is defined analogously for climatology. Note that only one of the parameters $z_{c,s,t}$ or $z_{p,s,t}$ could truly be 1; but for estimation these parameters can take on any value in the interval $[0, 1]$. Also, note $\hat{z}_{p,s,t} = 1 - \hat{z}_{c,s,t}$. Then the E-step is

$$\hat{z}_{p,s,t}^{(j)} = \frac{w^{(j-1)} a_s g_p(\gamma_{s,t}|f_{p,s,t})}{w^{(j-1)} a_s g_p(\gamma_{s,t}|f_{p,s,t}) + (1 - w^{(j-1)}) a_s g_c(\gamma_{s,t}|f_{c,s,t})}. \quad (13)$$

and the M-step is

$$w^{(j)} = \frac{\sum_t \sum_s a_s \hat{z}_{p,s,t}^{(j)}}{\sum_t \sum_s a_s} \quad (14)$$

for the j -th iteration. To avoid degeneracies, any (s, t) pairs where $g_p(y_{s,t}|f_{p,s,t}) = g_c(y_{s,t}|f_{c,s,t})$ are omitted from this maximization. Therefore, the denominator in Equation 14 may be unequal to the number of years in the training period. Throughout this post-processing, regions that are not well-represented by a contour (the beige regions in Figure 2) are assigned their climatology value. As such, they do not factor into the weights.

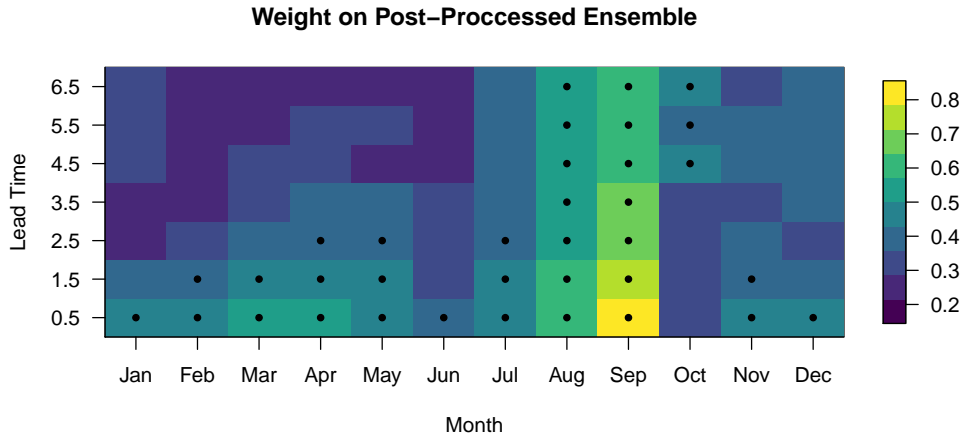


Figure 5: Weight on the post-processed ensemble model by month and lead time. A black dot indicates that the weight is at least 0.4. The post-processed ensemble gets more weight at short lead times and in the months leading up to the sea ice minimum. The weight on climatology is equal to one minus the weight on the post-processed ensemble.

Allowing the relative weight between the post-processed ensemble and climatology to vary over forecast month and lead time is a crucial feature in MCF’s performance. Figure 5 shows the average weight placed on the post-processed ensemble for the years in the test set. High weights typically occur at short lead times which reflects the fact that the ensemble typically has the most skill close to its initialization. High weights also occur in months leading up to the sea ice minimum in September. These are periods of high year-to-year variability, so climatology is likely to perform poorly and the ensemble’s ability to simulate evolving physical conditions takes on more importance.

4 Method evaluation

4.1 Evaluation set-up

We evaluate our post-processing methods on a 25-member ensemble from the European Centre for Medium-Range Weather Forecasts (ECMWF) (available from Copernicus Climate Change Service, 2019). Among a set of publicly-available ensembles without post-processing, ECMWF was shown to generally be most skillful (Zampieri et al., 2018). ECMWF forecasts are initialized monthly and extend 215 days. Model output was regridded to the National Snow and Ice Data Center Polar stereographic grid with approximately 25-km by 25-km grid (National Snow and Ice Data Center, 2017) using a nearest-neighbors method (Zhuang, 2018). Daily output was averaged to monthly to compare with a monthly observational prod-

uct produced from the National Aeronautics and Space Administration satellites Nimbus-7 SMMR and DMSP SSM/I-SSMIS and downloaded from the National Snow and Ice Data Center (Comiso, 2017). We report lead times treating the monthly mean as the halfway point within a month. For example, the 0.5-month lead forecast for January refers to the average of the first 31 days of a forecast initialized on January 1st. Grid boxes that are coded as land in the observations, the ensemble, or the *IceCast* R package (Director et al., 2019) are treated as land.

We assess forecasts for 2008-2016 for all months for seven lead times ranging from 0.5 to 6.5 months. Such forecasts made for the past are also known as a reforecast. The forecasts previously described are summarized in lines 1-4 of Table 1. All years preceding the forecast year beginning in 1993 are used in fitting Contour-Shifting. A 10-year rolling window is used to fit the statistical model for generating contours and a 3-year rolling window is used to determine the weights in MCF. Appendix F discusses training lengths further. One hundred contours are generated for each forecast.

We compare our results to two additional reference forecasts summarized in lines 5-6 of Table 1. Trend Adjusted Quantile Mapping (TAQM) is another recently-developed statistical post-processing method for sea ice (Dirkson et al., 2019). TAQM fits a parametric probability distribution to ensemble model output and applies a specialized version of quantile mapping to produce probabilistic forecasts of sea ice concentration. TAQM estimates the distribution of sea ice concentrations from which the probability of sea ice presence (concentration of at least 15%) can be obtained. We also compute a damped persistence forecast in a manner similar to Wayand et al. (2019). Damped persistence forecasts estimate the sea ice concentration in forecast month m using linear regression and the observed sea ice concentration in the initialization month i . For each grid box, the concentration for month m in year t , denoted $y_{m,t}$, is estimated as

$$\hat{y}_{m,t} = \hat{\beta}_m t + (y_i - \hat{\beta}_i t_i) \hat{\alpha}, \quad (15)$$

where $\hat{\beta}_m$ and $\hat{\beta}_i$ are the coefficients for linear regressions of y_m and y_i on year, respectively. The value $\hat{\alpha}$ is set to be the empirical correlation of y_m and y_i and is estimated from past observations. If all values of y_m and/or y_i in the training period are the same, the empirical correlation is undefined. In these cases, we set $\hat{\alpha}$ to 0, which makes Equation 15 equivalent to linear regression. When $i \leq m$, $t_i = t$, otherwise $t_i = t - 1$. Grid boxes with predicted concentration of at least 0.15 are forecasted to contain sea ice. Observations beginning in 1981 and extending up to the initialization time are used in fitting.

We evaluate calibration with reliability diagrams. These diagrams plot the forecasted probability of observing sea ice against the proportion of times sea ice was observed. A

Table 1: Summary of forecasts types evaluated. Probabilistic forecasts give estimates in the interval $[0, 1]$ and binary forecasts indicate predicted sea ice presence

Forecast	Probabilistic	Binary
Ensemble	proportion of ensemble members predicting sea ice	indicator if median ensemble member predicts sea ice
Post-Processed Ensemble	ensemble mean forecast bias-corrected with Contour-Shifting and calibrated by generating contours	ensemble mean forecast bias-corrected with Contour-Shifting
Climatology	proportion of observations in the 10 years preceding the forecast year that contain sea ice	indicator of if at least 5 of the 10 years preceding the forecast year contained sea ice
Mixture Contour Forecast (MCF)	forecast formed by weighting probability densities from climatology and the post-processed ensemble	indicator if forecast formed by weighting probability densities from climatology and the post-processed ensemble predicts sea ice with $p \geq 0.5$
Trend Adjusted Quantile Mapping (TAQM)	ensemble post-processed using technique in Dirkson et al. (2019)	NA
Damped Persistence	NA	indicator of if predicted sea ice concentration from a damped persistence forecast is at least 0.15 (modified from Wayand et al. (2019))

perfectly calibrated forecast would have all points on the $y = x$ line, i.e. grid boxes forecasted to contain sea ice with some probability actually contain sea ice that same proportion of the time. So, the closer the points lie to the $y = x$ line, the better calibrated the forecast is. We also evaluate forecast accuracy using Brier scores (Brier, 1950). We compute average area-weighted Brier scores over the $T = 9$ years in the test set as

$$\frac{\sum_t \sum_s a_s (f_{s,t} - o_{s,t})^2}{T}, \quad (16)$$

where $f_{s,t}$ and $o_{s,t}$ denote the forecast and observation in grid box s in year t respectively. The value a_s is the proportion of the total area in grid box s . The observed value is 1 when the sea ice concentration is at least 0.15, and 0 otherwise. For probabilistic forecasts, $f_{i,j} \in [0, 1]$ and for binary forecasts, $f_{i,j} \in \{0, 1\}$.

4.2 Forecast Assessment

Uncertainty information is needed for maritime planning to adequately evaluate risks and benefits. Like Gneiting et al. (2007), we consider accurate model calibration to be of paramount importance for issuing probabilistic forecasts. We illustrate the importance of calibration in this context with Figure 6, which shows samples of each of the probabilistic forecasts introduced in Section 3 for September 2008. The corresponding observed sea ice edge for September 2008 is also plotted for reference. Figure 6 illustrates the types of forecasting errors that can occur when forecasts are not calibrated. Specifically, events with low predicted probability occur more often than expected and/or events with high predicted probability occur less often than expected.

For MCF, the observed contour is almost entirely contained within regions with positive probability and has minimal area where sea ice is predicted with probability 1 but is not observed. In contrast, the observed contour more often goes through regions with zero probability for the ensemble and post-processed ensemble predictions. The climatology forecast has substantial area where sea ice is predicted with probability 1, but is not observed. The resulting discrepancy between the forecasted probability and what will likely occur make maritime planning and risk mitigation difficult.

We now evaluate model calibration for the probabilistic forecasts. Shipping varies seasonally in the Arctic, with more shipping in months around the annual sea ice minimum in September (Ellis and Brigham, 2009), so we emphasize performance in these peak-shipping months. In Figure 7 we show the reliability diagrams for the peak-shipping months for the probabilistic forecasts. Predictions from MCF are substantially better calibrated than the ensemble and better calibrated than TAQM during these months. Figures 13 and 14 in the appendix show that MCF always improves calibration over the unadjusted ensemble and generally improves calibration compared to TAQM, especially at short lead times. Overall, MCF provides better calibrated forecasts of the probability of sea ice presence than the raw ensemble or the ensemble after TAQM post-processing.

Conditional on issuing calibrated forecasts, forecasts with narrower intervals are desirable. In Figure 8, we plot the average Brier score in peak-shipping months by lead time for the probabilistic forecasts. The damped persistence forecast is also included as a reference, since at the shortest lead times, its performance is competitive with probabilistic forecasts. The ensemble forecasts typically have increasing Brier scores as lead time increases. Our contour post-processing improves forecast accuracy and MCF improves accuracy further. For these months, MCF typically provides the most accurate forecast, except at the shortest lead

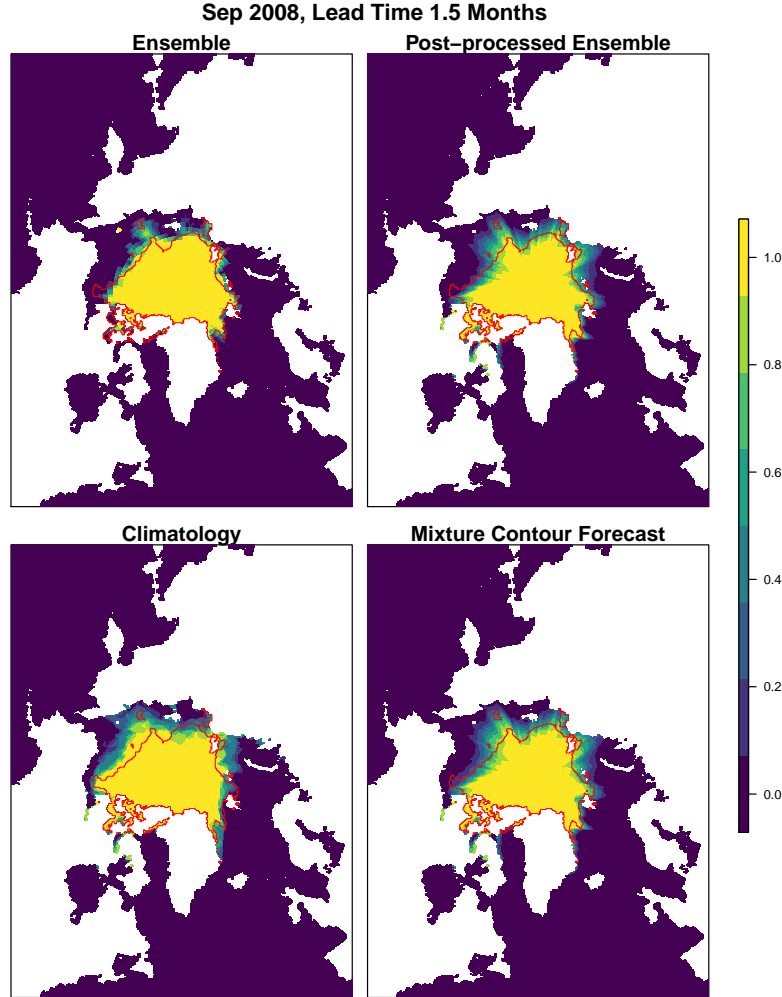


Figure 6: Forecasts of the probability of sea ice presence for September 2008 using different methods. Forecasts are described in Table 1. The red line is the observed sea ice edge contour and white areas are land. For MCF, the observed ice edge is almost completely within areas with positive probability and has little area where sea ice is predicted with probability 1, but is not observed. In contrast, the observed sea ice edge more often goes through regions with zero probability in the ensemble and post-processed ensemble forecasts. In the climatology forecast, there is considerable area where sea ice is predicted with probability 1 but is not observed.

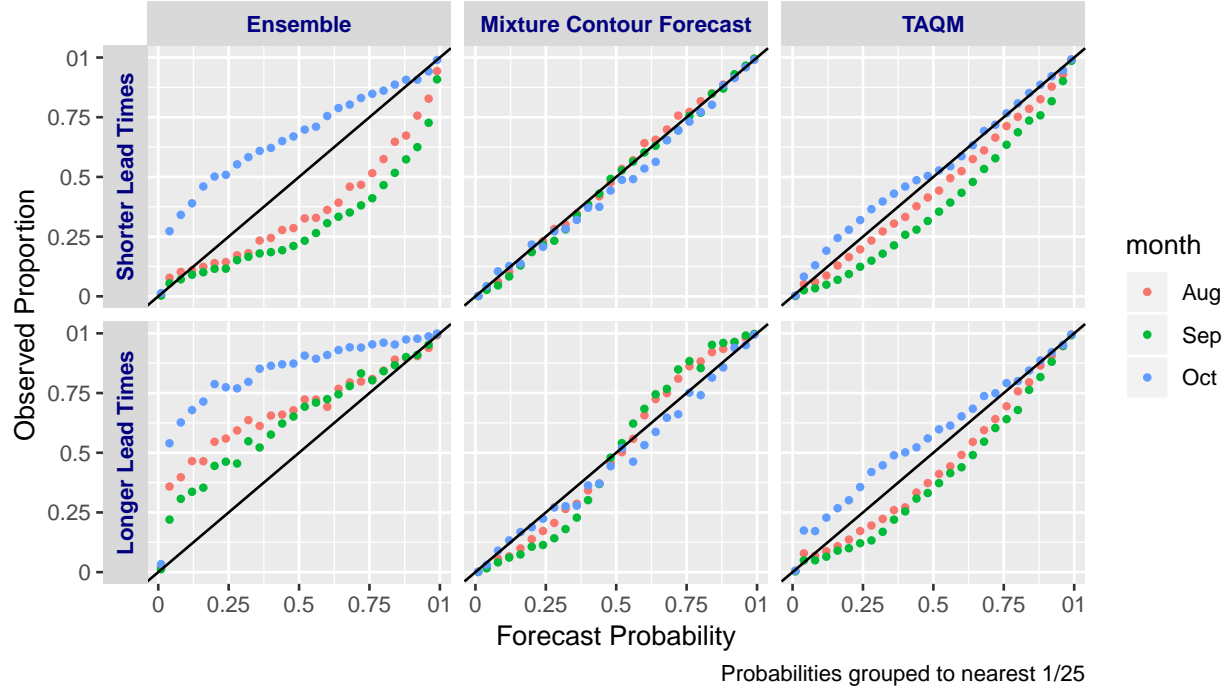


Figure 7: Plots of the average proportion of times sea ice was observed against predicted probability of sea ice presence for the raw ECMWF forecasts (left) and after post-processing with MCF (middle) and TAQM (right). Forecasts are grouped into lead times of 0.5 and 1.5 months (top) and 2.5-6.5 months (bottom). A perfectly calibrated forecast would have all points on the $y = x$ line.

time of 0.5 weeks. As lead time increases MCF’s performances converges to equal or better performance than climatology. TAQM also generally improves accuracy of forecasts.

Figures 10 and 11 in the appendix show that TAQM and MCF have similar overall accuracy, but the pattern of their performance by lead time and month varies. For peak shipping months, MCF outperforms TAQM, suggesting that our specialized modeling of the sea ice edge has benefits for maritime planning use. For other applications, more general techniques like TAQM may be more appropriate. For the shortest lead time of 0.5 months, the damped persistence forecast performs best, but its skill decays rapidly with lead time. The performance of the damped persistence forecast indicates that there could be a role for the the current observed state of the sea ice in forecasting, but that the role would need to be restricted to very short lead times. In summary, MCF provides the best calibrated forecasts year round and the most accurate forecasts during peak-shipping months.

We also briefly assess binary forecasts with Figure 9, which is analogous to Figure 8 except that it focuses on binary forecasts. Binary forecasts are inherently poorly-calibrated, and so are not optimal, but can be used to assess bias correction. The binary post-processed

ensemble improves accuracy compared to the ensemble. Binary MCF performs similarly to the binary post-processed ensemble in general, but MCF substantially outperforms the post-processed ensemble when the ensemble forecast is poor. This case illustrates that the adaptive weighting provided by MCF is valuable when issuing binary forecasts as well as probabilistic forecasts. Binary forecasts for all seasons are in Figure 10 in the appendix.

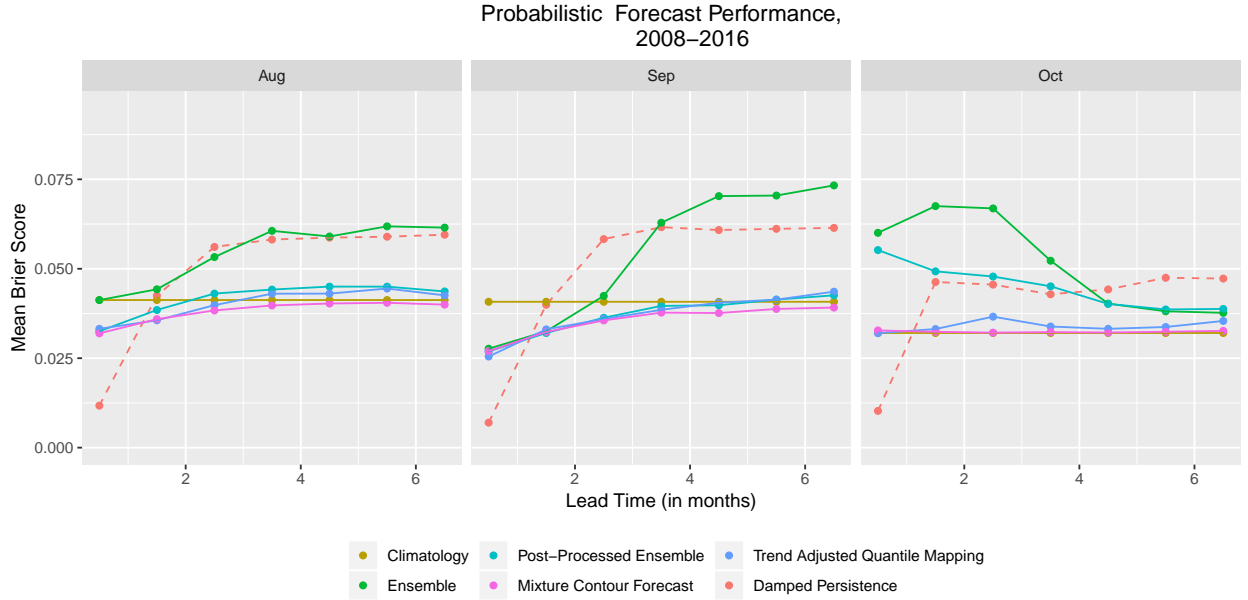


Figure 8: Average Brier scores by month for the test years 2008-2016 for the probabilistic forecasts and a damped persistence reference binary forecast. The Brier Score for each grid box is weighted based on its area. Forecasts are described in Table 1.

5 Discussion

We have introduced the Mixture Contour Forecasting method for issuing probabilistic sea ice forecasts. MCF forecasts are probabilistic and well-calibrated, meaning that their predicted probability of sea ice presence at a given location approximately matches the proportion of times sea ice will be observed at these locations. At most lead times and forecast months, probabilistic MCF forecasts are also as or more accurate than the raw ECMWF ensemble and the other post-processed and statistical forecasts. Because MCF provides well-calibrated and relatively-accurate forecasts, MCF’s use has the potential to increase operational forecasting skill of sea ice and thereby improve maritime planning in the Arctic.

We have also developed a novel framework for directly modeling contours. While forecasts could likely be made for sea ice concentration by modeling all the seas of the Arctic

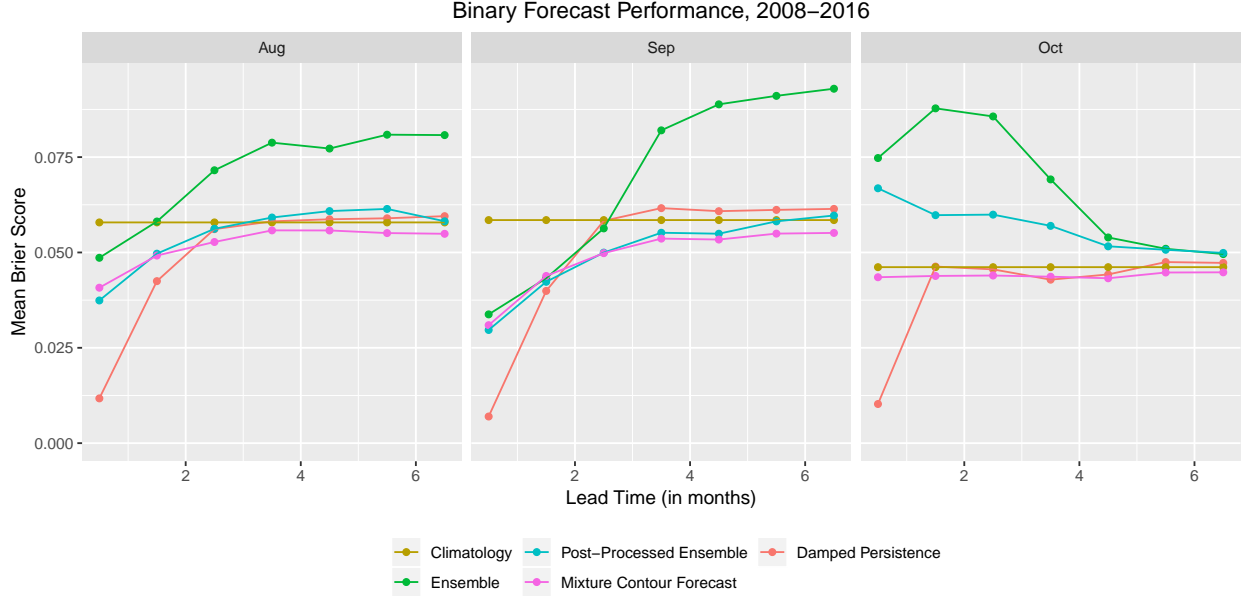


Figure 9: As in Figure 8, but for the binary forecasts.

with traditional field-based geostatistical models (e.g., Zimmerman and Stein, 2010) or by identifying the exceedance level contours estimated from fields (Bolin and Lindgren, 2015; French and Hoeting, 2016), these approaches are unlikely to be optimal for this application. The majority of the error in sea ice forecasts occurs in the region where a rapid transition from fully ice-covered regions to open water occurs (Tietsche et al., 2014). Whether sea ice will be found in grid boxes well into the interior of the sea ice region and far from the sea ice edge is essentially known in advance. So, placing the majority of the computational cost and modeling effort on the boundary is advantageous. MCF provides a framework for modeling that could be extended to other situations where the boundary is of interest.

As implemented in this paper, estimates of the covariance of the sea ice edge are based on the observed covariance of the preceding years. These estimates are therefore independent of the covariance of the sea ice edge in the ensemble members. However, the ensemble could plausibly give information about the expected covariance that could not be obtained from past observations. For example, sea ice is expected to continue to become thinner. Thinner sea ice is more affected by stochastic meteorological conditions, so the variance of sea ice extent will likely increase (Holland et al., 2011). These types of effects are captured by the ensemble, but are not in past observations. As such, incorporating the covariance in the ensemble could further improve forecast skill. Methods to do this will need to account for how the ensemble’s covariance and bias vary spatially and seasonally.

The ECMWF ensemble used in Section 4 is not the only ensemble prediction system.

The post-processing techniques developed in this paper could be directly applied to other ensembles, since they do not use any specific features of the ECMWF ensemble. However, model biases and calibration issues vary, so exact performance would need to be assessed. Different ensembles also vary moderately in which forecast months they perform well in and vary more substantially in how skill declines with lead time (Zampieri et al., 2018). So, extending MCF to use multiple ensembles as has been done for other meteorological variables could provide further skill (e.g., Raftery et al., 2005; Weigel et al., 2008).

The preceding analysis of sea ice forecasting highlights where statistical post-processing can provide value. Many aspects of physical processes are known to evolve following well-established equations. Such information can only be crudely approximated with a purely observational data-driven approach. On the other hand, physical models are often biased or poorly calibrated, and statistical post-processing methods can be effective in remedying these problems. Combining the strengths of physical and statistical modeling creates predictions that are more accurate than either modeling framework alone.

References

- Blanchard-Wrigglesworth, E., Cullather, R. I., Wang, W., Zhang, J., and Bitz, C. M. (2015). Model forecast skill and sensitivity to initial conditions in the seasonal Sea Ice Outlook. *Geophysical Research Letters*, 42(19):8042–8048.
- Bolin, D. and Lindgren, F. (2015). Excursion and contour uncertainty regions for latent gaussian models. *Journal of the Royal Statistical Society: Series B (Statistical Methodology)*, 77(1):85–106.
- Brier, G. (1950). Verification of forecasts expressed in terms of probability. *Monthly Weather Review*, 78(1):1–3.
- Bushuk, M., Msadek, R., Winton, M., Vecchi, G. A., Gudgel, R., Rosati, A., and Yang, X. (2017). Skillful regional prediction of Arctic sea ice on seasonal timescales. *Geophysical Research Letters*, 44(10):4953–4964.
- Cavalieri, D. J. and Parkinson, C. L. (2012). Arctic sea ice variability and trends, 1979-2010. *The Cryosphere*, 6(4):881.
- Chevallier, M., Salas y Mélia, D., Voldoire, A., Déqué, M., and Garric, G. (2013). Seasonal forecasts of the pan-Arctic sea ice extent using a GCM-based seasonal prediction system. *Journal of Climate*, 26(16):6092–6104.
- Comiso, J. (2017). Bootstrap sea ice concentrations from Nimbus-7 SMMR and DMSP SSM/I-SSMIS. version 3.
- Comiso, J. C., Parkinson, C. L., Gersten, R., and Stock, L. (2008). Accelerated decline in the Arctic sea ice cover. *Geophysical Research Letters*, 35(1).
- Copernicus Climate Change Service (2019). Copernicus climate change service climate data store. <https://cds.climate.copernicus.eu/cdsapp#!/home>.
- Dempster, A. P., Laird, N. M., and Rubin, D. B. (1977). Maximum likelihood from incomplete data via the EM algorithm. *Journal of the Royal Statistical Society: Series B (Methodological)*, 39(1):1–22.
- Director, H. M., Raftery, A. E., and Bitz, C. M. (2017). Improved sea ice forecasting through spatiotemporal bias correction. *Journal of Climate*, 30(23):9493–9510.
- Director, H. M., Raftery, A. E., and Bitz, C. M. (2019). *IceCast: Apply Statistical Post-Processing to Improve Sea Ice Predictions*. R package version 2.0.0.

- Dirkson, A., Merryfield, W. J., and Monahan, A. H. (2019). Calibrated probabilistic forecasts of Arctic sea ice concentration. *Journal of Climate*, 32(4):1251–1271.
- Douglas, D. H. and Peucker, T. K. (1973). Algorithms for the reduction of the number of points required to represent a digitized line or its caricature. *Cartographica: the international journal for geographic information and geovisualization*, 10(2):112–122.
- Eddelbuettel, D., François, R., Allaire, J., Ushey, K., Kou, Q., Russel, N., Chambers, J., and Bates, D. (2011). Rcpp: Seamless R and C++ integration. *Journal of Statistical Software*, 40(8):1–18.
- Eddelbuettel, D. and Sanderson, C. (2014). RcppArmadillo: Accelerating R with high-performance C++ linear algebra. *Computational Statistics & Data Analysis*, 71:1054–1063.
- Ellis, B. and Brigham, L. (2009). Arctic marine shipping assessment 2009 report.
- French, J. P. and Hoeting, J. A. (2016). Credible regions for exceedance sets of geostatistical data. *Environmetrics*, 27(1):4–14.
- Gelman, A. and Rubin, D. B. (1992). Inference from iterative simulation using multiple sequences. *Statistical Science*, 7(4):457–472.
- Gneiting, T. (2013). Strictly and non-strictly positive definite functions on spheres. *Bernoulli*, 19(4):1327–1349.
- Gneiting, T., Balabdaoui, F., and Raftery, A. E. (2007). Probabilistic forecasts, calibration and sharpness. *Journal of the Royal Statistical Society: Series B (Statistical Methodology)*, 69(2):243–268.
- Guemas, V., Blanchard-Wrigglesworth, E., Chevallier, M., Day, J. J., Déqué, M., Doblas-Reyes, F. J., Fučkar, N. S., Germe, A., Hawkins, E., Keeley, S., et al. (2016). A review on Arctic sea-ice predictability and prediction on seasonal to decadal time-scales. *Quarterly Journal of the Royal Meteorological Society*, 142(695):546–561.
- Hoff, P. D. (2009). *A First Course in Bayesian Statistical Methods*. Springer Texts in Statistics. Springer New York, New York, NY.
- Holland, M. M., Bailey, D. A., and Vavrus, S. (2011). Inherent sea ice predictability in the rapidly changing Arctic environment of the Community Climate System Model, version 3. *Climate Dynamics*, 36(7-8):1239–1253.

- Huber, P. J. (2011). *Robust Statistics*. Springer.
- Melia, N., Haines, K., and Hawkins, E. (2016). Sea ice decline and 21st century trans-Arctic shipping routes. *Geophysical Research Letters*, 43(18):9720–9728.
- Msadek, R., Vecchi, G. A., Winton, M., and Gudgel, R. G. (2014). Importance of initial conditions in seasonal predictions of Arctic sea ice extent. *Geophysical Research Letters*, 41(14):5208–5215.
- National Snow and Ice Data Center (2017). Region mask for the Northern Hemisphere. http://nsidc.org/data/polar-stereo/tools_masks.html.
- Plummer, M., Best, N., Cowles, K., and Vines, K. (2006). Coda: Convergence diagnosis and output analysis for mcmc. *R News*, 6(1):7–11.
- Raftery, A. E., Gneiting, T., Balabdaoui, F., and Polakowski, M. (2005). Using Bayesian model averaging to calibrate forecast ensembles. *Monthly Weather Review*, 133(5):1155–1174.
- Raftery, A. E. and Lewis, S. M. (1992). Practical Markov chain Monte Carlo: comment: one long run with diagnostics: implementation strategies for Markov chain Monte Carlo. *Statistical Science*, 7(4):493–497.
- Raftery, A. E. and Lewis, S. M. (1995). The number of iterations, convergence diagnostics and generic metropolis algorithms. *Practical Markov Chain Monte Carlo*, 7(98):763–773.
- Sigmond, M., Fyfe, J. C., Flato, G. M., Kharin, V. V., and Merryfield, W. J. (2013). Seasonal forecast skill of Arctic sea ice area in a dynamical forecast system. *Geophysical Research Letters*, 40(3):529–534.
- Smith, L. C. and Stephenson, S. R. (2013). New Trans-Arctic shipping routes navigable by midcentury. *Proceedings of the National Academy of Sciences*, 110(13):E1191–E1195.
- Stroeve, J. C., Serreze, M. C., Holland, M. M., Kay, J. E., Malanik, J., and Barrett, A. P. (2012). The Arctic’s rapidly shrinking sea ice cover: a research synthesis. *Climatic Change*, 110(3-4):1005–1027.
- Tietsche, S., Day, J. J., Guemas, V., Hurlin, W. J., Keeley, S. P. E., Matei, D., Msadek, R., Collins, M., and Hawkins, E. (2014). Seasonal to interannual Arctic sea ice predictability in current global climate models. *Geophysical Research Letters*, 41(3):1035–1043.

- Tobin, J. (1958). Estimation of relationships for limited dependent variables. *Econometrica: journal of the Econometric Society*, pages 24–36.
- Wang, W., Chen, M., and Kumar, A. (2013). Seasonal prediction of Arctic sea ice extent from a coupled dynamical forecast system. *Monthly Weather Review*, 141(4):1375–1394.
- Wayand, N. E., Bitz, C. M., and Blanchard-Wrigglesworth, E. (2019). A year-round subseasonal-to-seasonal sea ice prediction portal. *Geophysical Research Letters*, 46(6):3298–3307.
- Weigel, A. P., Liniger, M. A., and Appenzeller, C. (2008). Can multi-model combination really enhance the prediction skill of probabilistic ensemble forecasts? *Quarterly Journal of the Royal Meteorological Society*, 134(630):241–260.
- Wolfinger, R. D. (1996). Heterogeneous variance: covariance structures for repeated measures. *Journal of Agricultural, Biological, and Environmental Statistics*, pages 205–230.
- Zampieri, L., Goessling, H. F., and Jung, T. (2018). Bright prospects for Arctic sea ice prediction on subseasonal time scales. *Geophysical Research Letters*, 45(18):9731–9738.
- Zhang, B. and Cressie, N. (2019). Estimating spatial changes over time of Arctic Sea ice using hidden 2×2 tables. *Journal of Time Series Analysis*, 40(3):288–311.
- Zhuang, J. (2018). xesmf: Universal regridding for geospatial data.
- Zimmerman, D. L. and Stein, M. L. (2010). Classical geostatistical methods. In Gelfand, A. E., Diggle, P., Guttorp, P., and Fuentes, M., editors, *Handbook of Spatial Statistics*, pages 29–44. CRC Press: Boca Raton, FL.

Appendices

A Standard deviation corresponding to γ proportion of mass of a Gaussian within symmetric bounds

Consider a Gaussian distribution with known mean $\mu = (m+M)/2$. The standard deviation, $\sigma > 0$, such that $100 \times \gamma$ percent of the mass of the distribution is within m and M is

$$\sigma = \frac{(M - m)/2}{\Phi^{-1}(1 + \gamma/2)} \quad (17)$$

where $\gamma \in (0, 1)$ and $\Phi^{-1}(\cdot)$ is the standard normal inverse cumulative distribution function.

Proof. Let X be a random variable with $X \sim N(\mu, \sigma)$. Note that $\Pr(m \leq X \leq M) = \gamma$ is equivalent to $\Pr(x \leq M) = (1 - \gamma)/2 + \gamma = (1 + \gamma)/2$. Then,

$$\Pr\left(Z \leq \frac{M - (M + m)/2}{\sigma}\right) = \Pr\left(Z \leq \frac{(M - m)/2}{\sigma}\right) = \frac{1 + \gamma}{2}$$

Hence,

$$\frac{(M - m)/2}{\sigma} = \Phi^{-1}\left(\frac{1 + \gamma}{2}\right). \quad (18)$$

□

B Posterior distribution given partially observed \mathbf{X}

The posterior distribution introduced in Section 2.2.3 follows using Baye's rule and elementary probability:

$$\begin{aligned} p(\mu, \sigma, \rho, \mathbf{X}^u | \mathbf{X}^o) &\propto p(\mathbf{X}^o | \mu, \sigma, \rho, \mathbf{X}^u) p(\mu, \sigma, \rho, \mathbf{X}^u) \\ &= p(\mathbf{X}^o | \mu, \sigma, \rho, \mathbf{X}^u) p(\mathbf{X}^u | \mu, \sigma, \rho) p(\mu) p(\sigma) p(\rho) \\ &= \prod_{j=1}^N \{p(X_j^o | \mu, \sigma, \rho, X_j^u)\} \prod_{j=1}^N \{p(X_j^u | \mu, \sigma, \rho)\} p(\mu, \sigma, \rho) \\ &= \prod_{j=1}^N \{p(X_j^o | \mu, \sigma, \rho, X_j^u) p(X_j^u | \mu, \sigma, \rho)\} p(\mu) p(\sigma) p(\rho) \\ &= \prod_{j=1}^N \{p(X_j^o, X_j^u | \mu, \sigma, \rho)\} p(\mu) p(\sigma) p(\rho) \\ &= \prod_{j=1}^N \{p(X_j | \mu, \sigma, \rho)\} p(\mu) p(\sigma) p(\rho). \end{aligned} \quad (19)$$

C Additional figures

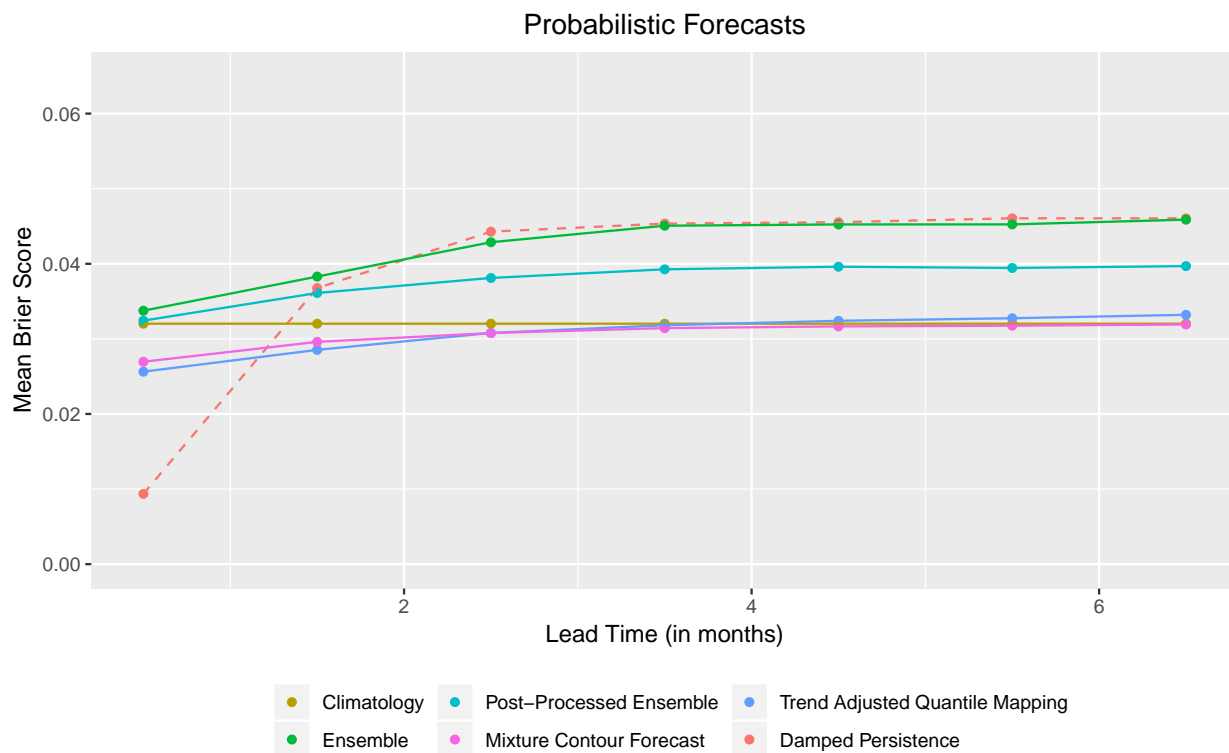


Figure 10: Overall Brier scores for the test years 2008-2016 for the probabilistic forecasts and a damped persistence reference binary forecast. The Brier Score for each grid box is weighted based on its area. Forecasts are described in Table 1 in the main text.

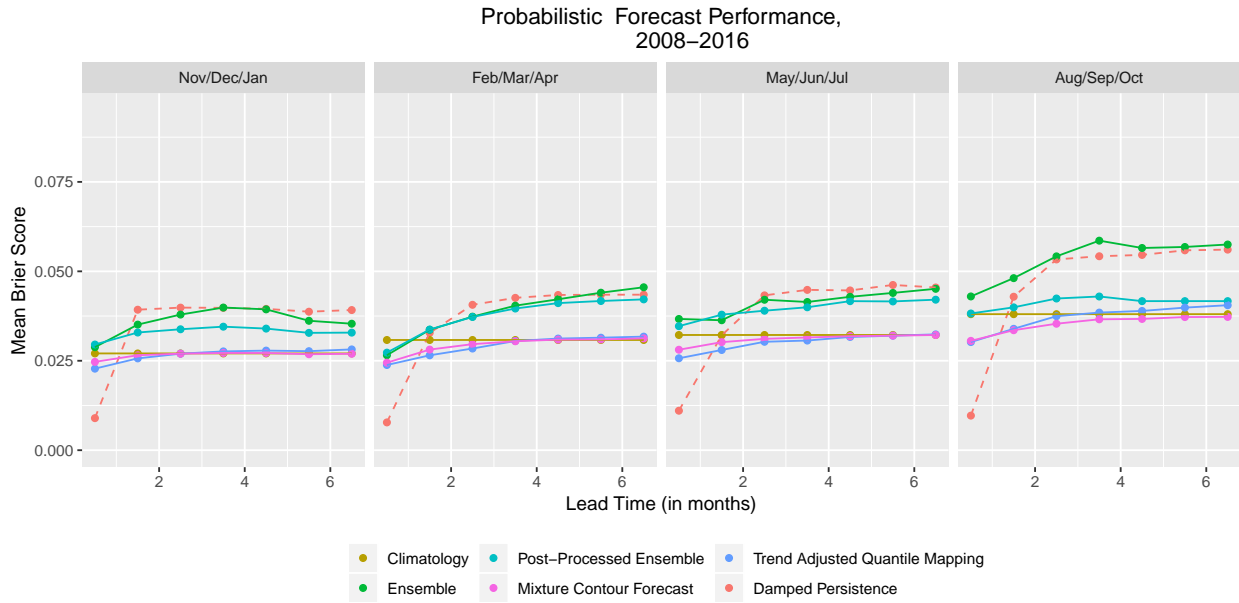


Figure 11: Average Brier scores grouped into three-month sets for the test years 2008-2016 for the probabilistic forecasts and a damped persistence reference binary forecast. The Brier Score for each grid box is weighted based on its area. Forecasts are described in Table 1 in the main text.

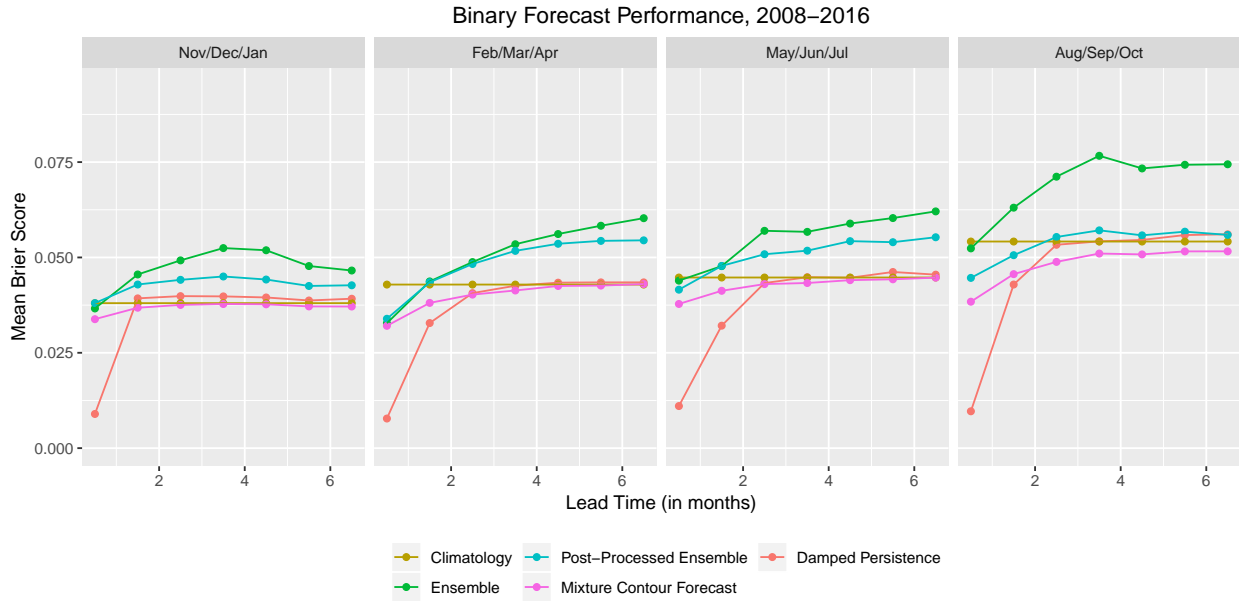


Figure 12: As in Figure 11, except for binary forecasts.

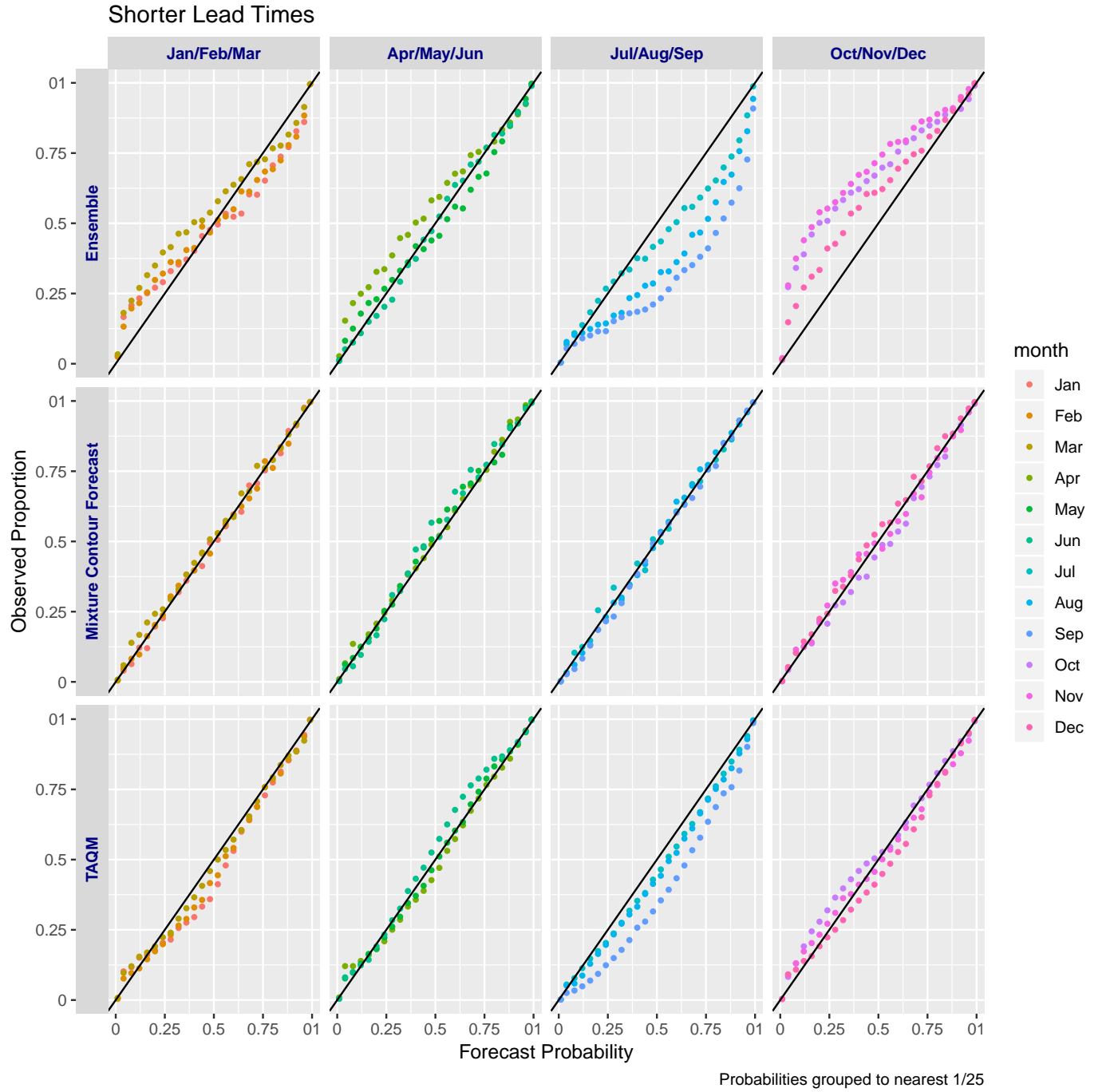


Figure 13: Plots of the average proportion of times sea ice was observed against the predicted probability of observing sea ice for the unadjusted ECMWF forecasts (top) and post-processed with MCF (middle) and TAQM (bottom) for lead times of 0.5 - 1.5 months. Results are grouped into three-month sets and all grid boxes are equally weighted.

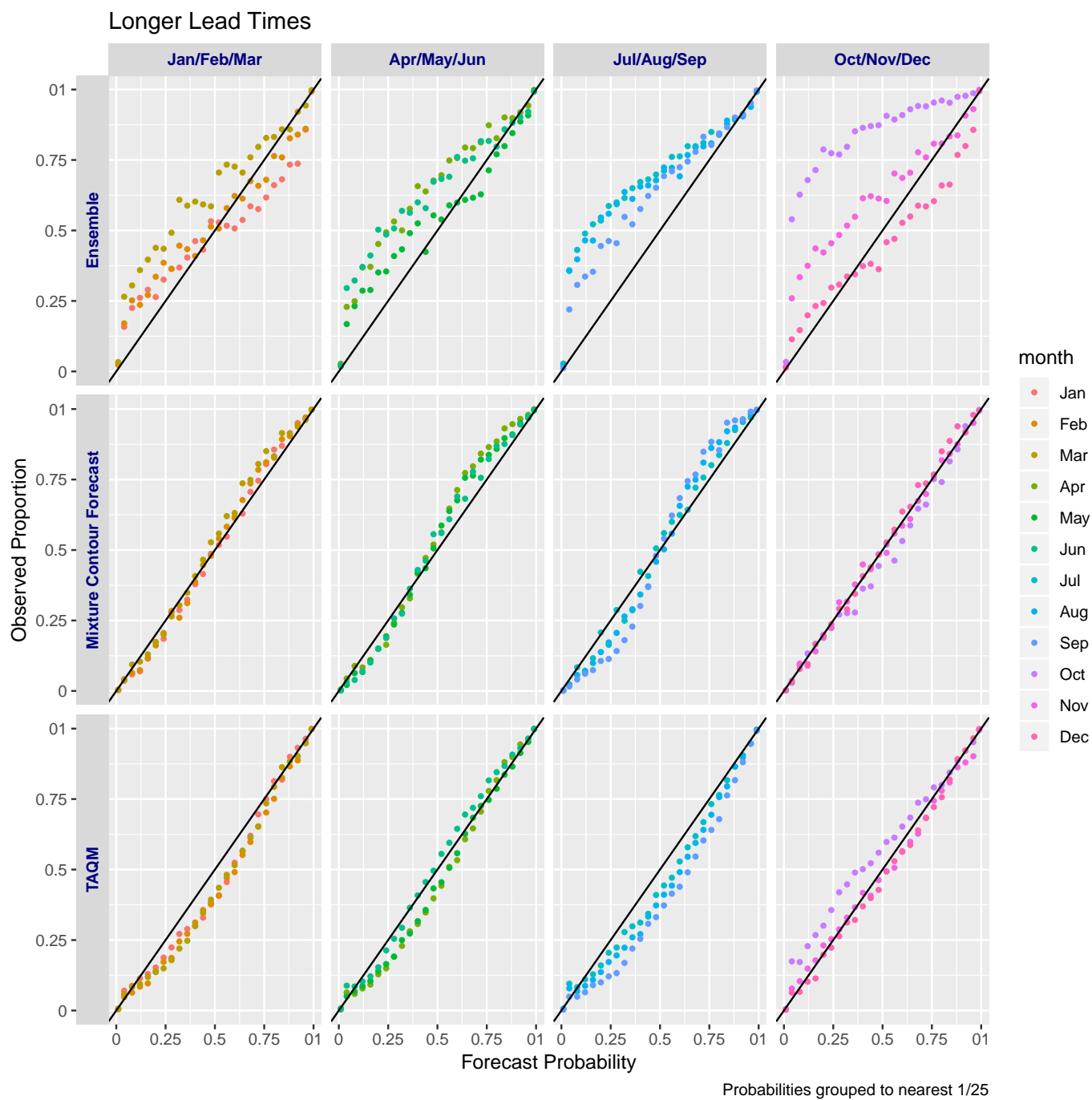


Figure 14: As in Figure 13 but for lead times of 2.5 - 6.5 months.

D MCMC Algorithm

To sample from the posterior distribution derived in Section 2.2.3 of the main text, we use a combination of Metropolis and Gibbs steps. In this section, we describe each step of the algorithm in detail. The algorithm is implemented in the *IceCast* R package with the `fit_cont_pars` function (Director et al., 2019).

D.1 Metropolis step for each $x_{ij}^u \in \mathbf{X}^u$

Each element, x_{ij}^u in vector X_j is sampled independently. On iteration t , we use the Normal proposal

$$x_{ij,t}^u \sim N(x_{ij,t-1}^u, \sigma_{x_{ij}^u}^2). \quad (20)$$

From the observed value y_{ij} and Equation 8 in the main text, the upper and lower bound for each x_{ij} are known. If they are both finite, the step size $\sigma_{x_{ij}^u}$ is set to be (1/150)-th of their range. Otherwise, $\sigma_{x_{ij}^u}$ is set to 0.03. Proposals outside the bounds for x_{ij}^u are automatically rejected. Otherwise, the log acceptance rate is

$$\log r \propto -\frac{1}{2}X_{j,t}^T \Sigma^{-1} X_{j,t}^t + X_{j,t}^T \Sigma^{-1} \mu + \frac{1}{2}X_{j,t-1}^T \Sigma^{-1} X_{j,t-1}^t - X_{j,t-1}^T \Sigma^{-1} \mu \quad (21)$$

where $X_{j,t}$ is the vector with the proposed value $x_{ij,t}^u$ used for x_{ij}^u .

D.2 Gibbs step for μ

For updating μ , \mathbf{X} can temporarily be treated as fully observed. Then, following Hoff (2009, p. 107-108), we have the full conditional

$$p(\mu | \mathbf{X}, \Sigma, \rho) \sim N(\mu | \boldsymbol{\mu}^n, \Lambda^n) \quad (22)$$

where

$$\boldsymbol{\mu}^n = (\Lambda_0^{-1} + n\Sigma^{-1})^{-1} (\Lambda_0^{-1}\mu_0 + n\Sigma^{-1}\bar{\mathbf{X}}) \quad (23)$$

and

$$\Lambda^n = (\Lambda_0^{-1} + n\Sigma^{-1})^{-1} \quad (24)$$

with vector $\bar{\mathbf{X}} = \frac{1}{n} \sum_{j=1}^n X_j$. On each iteration, we can update μ with a Gibbs step accordingly.

D.3 Metropolis steps for σ

To balance good mixing and computation time, we sample the values for σ in groups. Sets of σ 's with corresponding lines in \mathbf{L} that are close together are grouped together, since their values are likely to be similar. The σ 's corresponding to contiguous groups of lines whose lengths y_i have zero variance in the observed years are always put together. All other σ 's are put in contiguous groups of no more than 25.

Let g denote the indices of some subset of the σ values and let g^c denote the complement of these indices. Further, let $\sigma = (\sigma_g, \sigma_{g^c})$. We use a multivariate normal proposal to sample the set σ_g . For iteration t ,

$$\sigma_{g,t} \sim N(\sigma_{g,t-1}, \Sigma_{\sigma,g}) \quad (25)$$

where $\Sigma_{\sigma,g}$ is a diagonal covariance matrix. In our implementation, the i -th diagonal element is set to be $(1/20)$ -th the standard deviation of all y_i 's unless that value is zero. In such cases, it is set to 0.1. The corresponding log acceptance rate is

$$\begin{aligned} \log r_{\sigma_g} = & -\frac{n}{2} \log |\Sigma(\rho, \sigma_t)| - \frac{1}{2} \sum_{j=1}^n X_j^T \Sigma^{-1}(\rho, \sigma_t) X_j + \sum_{j=1}^n X_j^T \Sigma^{-1}(\rho, \sigma_t) \boldsymbol{\mu} \\ & - \frac{n}{2} \boldsymbol{\mu}^T \Sigma^{-1}(\rho, \sigma_t) \boldsymbol{\mu} \\ & + \frac{n}{2} \log |\Sigma(\rho, \sigma_{t-1})| + \frac{1}{2} \sum_{j=1}^n X_j^T \Sigma^{-1}(\rho, \sigma) \mathbf{x}_i - \sum_{j=1}^n X_j^T \Sigma^{-1}(\rho, \sigma_{t-1}) \boldsymbol{\mu} \\ & + \frac{n}{2} \boldsymbol{\mu}^T \Sigma^{-1}(\rho, \sigma_{t-1}) \boldsymbol{\mu}. \end{aligned} \quad (26)$$

D.4 Metropolis step for ρ

We use a normal proposal for ρ . Specifically, on iteration t ,

$$\rho_t \sim N(\rho_{t-1}, \sigma_\rho^2) \quad (27)$$

where the step size, σ_ρ , is set to 0.01 in our implementation. The corresponding log acceptance rate is

$$\begin{aligned}
\log r_\rho = & -\frac{n}{2} \log |\Sigma(\rho_t, \sigma)| - \frac{1}{2} \sum_{j=1}^n X_j^T \Sigma^{-1}(\rho_t, \sigma) X_j + \sum_{j=1}^n X_j^T \Sigma^{-1}(\rho_t, \sigma) \mu \\
& - \frac{n}{2} \mu^T \Sigma^{-1}(\rho_t, \sigma) \mu \\
& + \frac{n}{2} \log |\Sigma(\rho_{t-1}, \sigma)| + \frac{1}{2} \sum_{i=1}^n X_j^T \Sigma^{-1}(\rho_{t-1}, \sigma) X_j - \sum_{i=1}^n X_j^T \Sigma^{-1}(\rho_{t-1}, \sigma) \mu \\
& + \frac{n}{2} \mu^T \Sigma^{-1}(\rho_{t-1}, \sigma) \mu.
\end{aligned} \tag{28}$$

D.5 Initialization

Because the model is high-dimensional, the Markov chain must be initialized near the posterior of the distribution or convergence will not occur in a reasonable length time. However, since the observed \mathbf{Y} are quite similar to the unobserved \mathbf{X} , the plug-in estimators obtained from \mathbf{Y} can be used to obtain reasonable initial estimates for some parameters. As such, we initialize the chain with

$$\mu_{i,0} := \sum_{j=1}^N Y_{ij} \tag{29}$$

$$x_{ij,0}^u := y_{ij} \tag{30}$$

$$\sigma_{i,0} := \begin{cases} SD(Y_i) & .05\epsilon < SD(Y_i) < 0.95b_i \\ .2(b_i - \epsilon) & \text{otherwise} \end{cases} \tag{31}$$

where the 0 subscript indicates the 0-th iteration and $SD(\cdot)$ is the standard deviation function. The values ϵ and b_i are the bounds for the uniform prior on σ_i as in Equation 5 in the main text. The second case for σ_i is used to avoid the poor mixing that results from having parameters start very close to their boundary. Since we have no information about ρ , we initialize it at the middle of its possible range

$$\rho_{i,0} = 0.5. \tag{32}$$

In practice, after the parameters for a single forecast have been sampled, it is reasonable to assume that the parameters for the next year's forecast will be very similar. So, in operational use, another option would be to initialize the parameters at the previous years' mean parameter value. The training periods are set as a rolling window, so the previous year's estimates are likely to be quite close to accurate initially, creating an effective warm start for the sampler.

D.6 Implementation

For all results in this paper, we use 2.5 million iterations of the MCMC chain. The first 500,000 iterations are set aside as burn-in. To save memory, we thin the chain and retain only the samples from every 50th iteration. The sampler is called from the `fit_cont_pars` function in the *IceCast* R package (Director et al., 2019). The Rcpp (Eddelbuettel et al., 2011) and RcppArmadillo (Eddelbuettel and Sanderson, 2014) are used for efficiency. Running this chain for all regions of the Arctic for a given forecast month takes between 1 and 4 days on a single core. How many regions need to be fit, how many unobserved values are in \mathbf{X} , the computer specifications, and other factors contribute to this variability.

E MCMC diagnostics

As in all MCMC, diagnostic analysis is needed to determine the appropriate chain length. We selected the number iterations to run the sampler by considering traceplots and model diagnostics for sample forecast months. In this Section, we evaluate one month in detail. Our analysis serves a dual purpose. It demonstrates that the number of iterations used in this paper’s analysis is reasonable and serves as a model for how MCMC diagnostics could be applied for future results obtained with this method.

We note that our primary goal in this paper is prediction and not inference and that only the mean of each parameter distribution is used. So, only reasonable sampling from the posterior distribution is needed for good performance. Therefore, we have not repeated this analysis on every forecast month and year. However, if our goals were to shift to inference on the parameter distributions, we would recommend doing a more thorough evaluation that would involve all parameters in each forecast month and year. We would also recommend repeating this initial diagnostic analysis if major changes are made to the method, such as changing the ensemble model used.

E.1 Sample Evaluation: September 2005

We evaluate the chains for September 2005 using the training years of 1995-2004. We selected this month as a sample, since the location of the sea ice edge is highly variable at this time of year. The model parameters are consequently likely to have high variability and need more iterations for fitting. Many other months could likely be fit adequately with less iterations.

Three regions contain sea ice in September 2005 and have a contour model fit for them: the Central Arctic, Baffin Bay, and Greenland Sea. Using the *coda* R package (Plummer et al., 2006), we compute the Raftery and Lewis Diagnostic (Raftery and Lewis, 1992, 1995)

for ρ , all μ_i and most values of σ_i . We use $r = 0.0125$ and report the maximum number of iterations needed after assessing both $q = 0.025$ and $q = 0.975$. In Tables 2 and Tables 3, we report the 50-th, 85-th, and 100-th percentiles of the estimated number of iterations needed from all μ_i and σ_i for each region. We omit from this analysis some chains for σ_i when more than 95% of the samples are within 3 units of one of its boundaries. This omission, or something similar, is needed because in some cases the parameter value that maximizes the posterior is on the boundary of the range. The chain will correctly not move or move little in such cases and the Raftery and Lewis Diagnostic does not make sense. In Table 4, we report the estimated number of iterations needed for ρ for the three regions.

Table 2: The 50-th, 85-th, and 100-th percentile for the estimated chain lengths for μ_i obtained from the Raftery and Lewis Diagnostic for the three regions evaluated.

Region	$n_{est,50}$	$n_{est,85}$	$n_{est,100}$
Central Arctic	48360	63390	123840
Baffin Bay	12300	12423	332160
Greenland Sea	26160	40764	87720

Table 3: As in Table 2, except for σ_i

Region	$n_{est,50}$	$n_{est,85}$	$n_{est,100}$
Central Arctic	275110	490173	1370880
Baffin Bay	231120	876544	1924320
Greenland Sea	277760	460620	649420

Table 4: Estimated chain lengths from the Raftery and Lewis Diagnostic for ρ

Region	n_{est}
Central Arctic	26376
Baffin Bay	1926
Greenland Sea	13490

In Figure 15, we show the traceplot for a typical chain for μ_i for each of the three regions. Figure 16 is an analogous figure for a typical σ_i . We selected the index i in each case by finding the chain with the estimated sample size closest to the median estimated number of iterations needed for all indices. Finally, Figure 17 shows the traceplots for ρ for the three regions.

The traceplots illustrate that the chains for ρ converge quite quickly and that the chains for μ start out at approximately the correct value. The σ_i parameters are slowest to converge and so determine how many iterations are needed. The traceplots also show that the burn-in of 500,000 is sufficient for the chains to have reached their posterior density region. Combined with the maximal value from the Raftery and Lewis diagnostic being approximately 1.9 million, these results indicate that the sample size of 2 million used in this paper is appropriate.

Because initialization is necessary as discussed in Section D.5 of the appendix, evaluation techniques such as the Gelman-Rubin diagnostic (Gelman and Rubin, 1992), which consider multiple chains initialized at different values, are not appropriate and so are not evaluated.

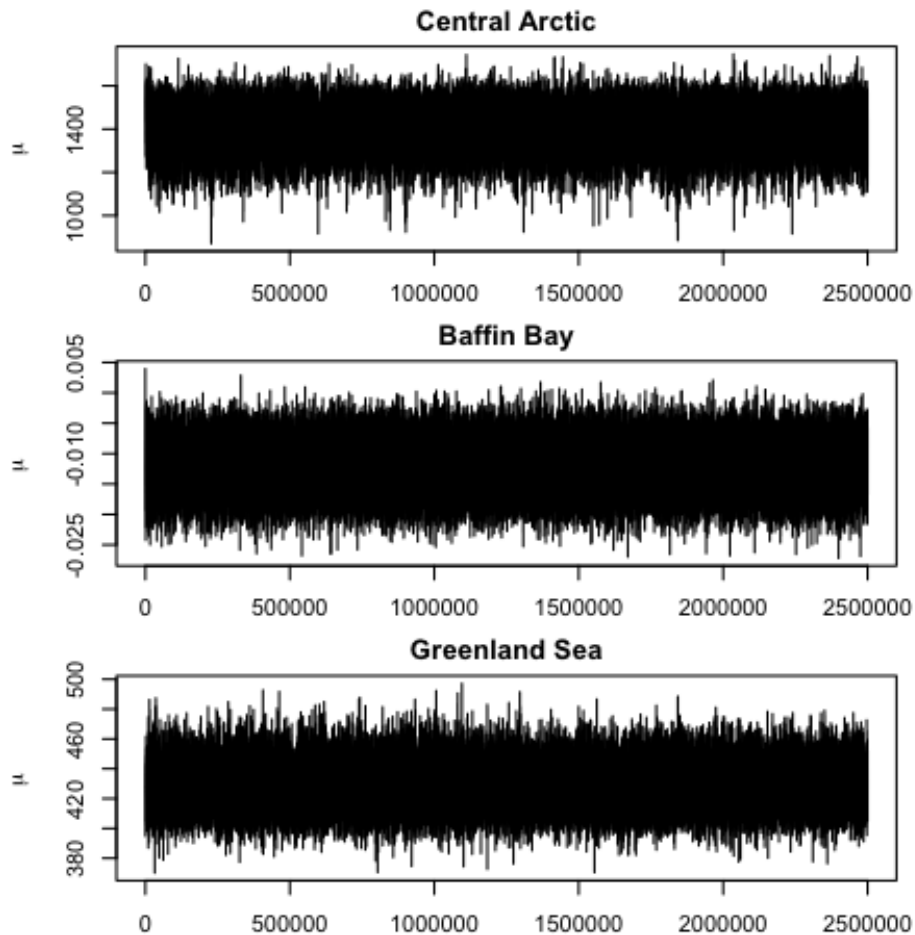


Figure 15: Traceplots for the chains in each of the three evaluated regions for a typical μ_i .

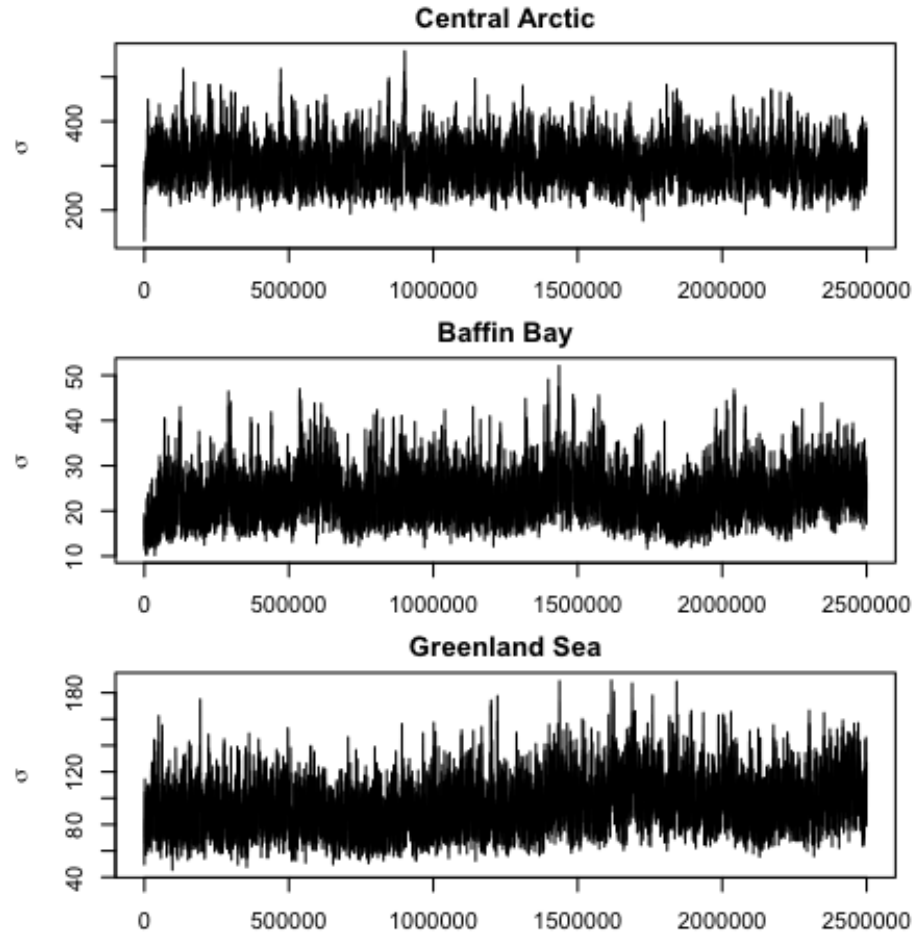


Figure 16: Traceplots for the chains in each of the three evaluated regions for a typical σ_i .

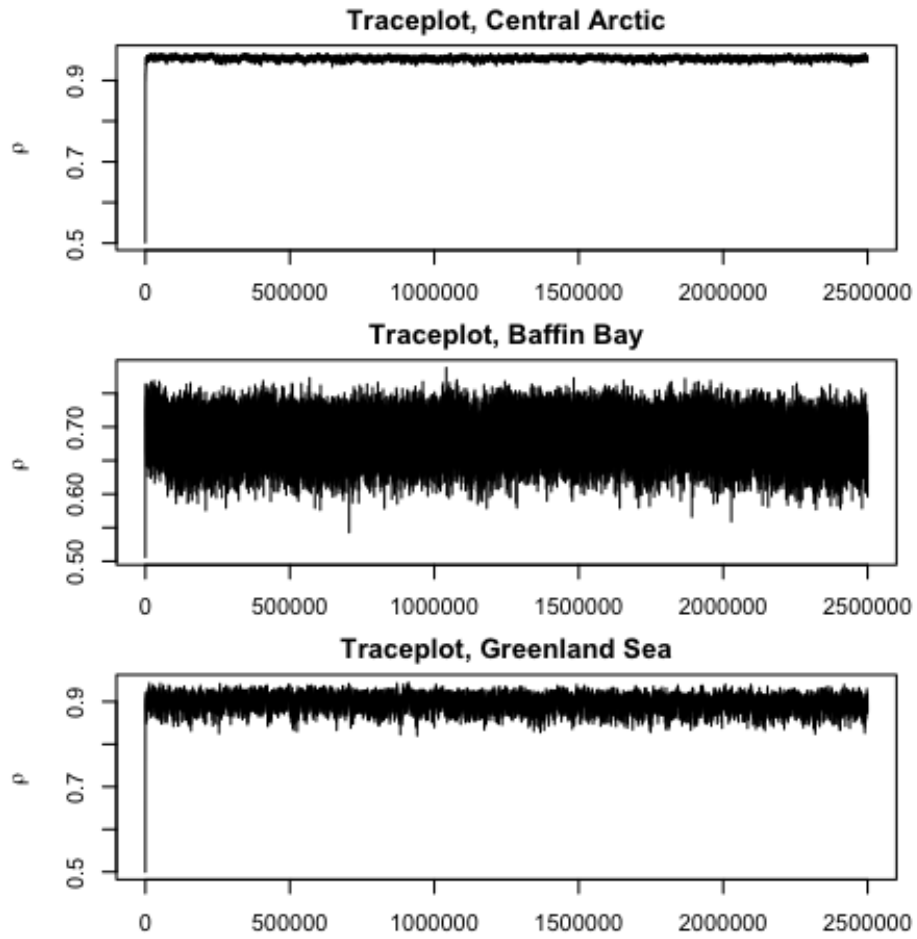


Figure 17: Traceplots for the parameter ρ in the three evaluated regions.

F Length of Training Periods

Several aspects of the modeling in this paper rely on fitting parameters using multiple previous years of data as a training period. Since the Arctic is changing, more recent data is likely to be more relevant, but using only a small number of years of data may lead to parameter estimates that are too variable. Computational cost and limited amounts of data further constrain the training lengths possible. So, determining the appropriate training window length is not obvious. In this section, we discuss our rationale for the values used in the paper.

Because Contour-Shifting explicitly models the time trend, we follow Director et al. (2017) and use all available data prior to the forecast year to fit the bias correction. So, using all available data gives more information about the trend. The earliest ensemble output available on the Copernicus Climate Change Service Climate Data Store (Copernicus Climate Change Service, 2019) is for 1993, so that is the earliest year used in fitting Contour-Shifting

The damped persistence forecast also relies on a trend. So, we use all available training data in fitting. Since this method only requires observations and they are available for earlier years than ensemble output, we fit this model with data beginning in 1981.

For the contour model used in post-processing, we elect to use 10 years of training data in a rolling window to fit each forecast month. We find in practice that this training length provides a good balance between recency and sufficient length. Given the relatively high computational cost of fitting these models and the need to have enough data set aside for the overall test set, we did not do a formal cross-validation of this result. Further analysis of these lengths would be of interest, particularly since the optimal training length might vary between forecast months.

In the paper, we use only three years of training data in a rolling window to fit the weights in the mixture. Since the weights are dependent on results after post-processing, there is not enough data to do a proper cross validation while leaving aside a reliable enough test set. We find three years works well in practice, but it is not clear this is optimal. For future use, we now evaluate the performance of different training lengths for the rolling window. We fit the weights and corresponding MCF forecasts for the years 2012-2016 using rolling windows of training lengths from 1-7 years. We report the mean Brier score over months and years. As in the main paper, we weight the grid boxes by their area. We find that a five-year training period performs best and would recommend this training length for operational use. We do note however that forecast performance does not appear to be particularly sensitive to this choice.

Table 5: Mean area-weighted Brier scores for MCF on the test set of 2012-2016 for different numbers of years of training data are used to determine the weight on the climatology versus the post-processed ensemble.

Years	Mean Brier Score
1	0.03181
2	0.03180
3	0.03177
4	0.03166
5	0.03156
6	0.03160
7	0.03164